Bulletin of the Seismological Society of America, Vol. 103, No. 1, pp. 463–486, February 2013, doi: 10.1785/0120120123

Shallow-Focus Repeating Earthquakes in the Tonga–Kermadec–Vanuatu Subduction Zones

by Wen-che Yu

Abstract This paper examines moderate shallow-focus repeating earthquakes along the Tonga–Kermadec–Vanuatu subduction zones by cross-correlating teleseismically recorded waveforms. A total of 23 clusters and 31 doublets are identified with an average cross-correlation coefficient of >0.8. A master-event algorithm is used to determine the precise relative locations. I then estimate and superpose the source areas among these event pairs. This analysis reveals that most of these correlated pairs are repeating earthquakes, which have similar seismic moments (M_0) and completely overlapping source areas. Most of the moderate repeating earthquakes were quasi-periodic with a recurrence interval (T_r) on the order of years, and occurred at the plate interface. The repeating earthquakes are used to study spatial–temporal variations in fault-slip rate ($\dot{d}$) and interplate coupling. Apart from spatial variations in $\dot{d}$, a temporal acceleration in $\dot{d}$ is observed, associated with large interplate earthquakes in the Vanuatu region. Interplate coupling is weak for most of the study areas, except the northern section 15°–19° S of the Tonga arc. Strong coupling in the northern Tonga interplate region appears to be at odds with the decoupling expected of a region associated with active back-arc extension. Repeating earthquakes are also used to examine the scaling relationship between M_0 and T_r derived from the San Andreas fault (SAF). The $T_r - M_0$ scaling relationship derived from the SAF can adequately account for the normalized T_r for the Kermadec, Vanuatu, and Tonga interplate regions where it is decoupled, suggesting that the convergence rate is the predominant influence on the recurrence interval in a repeating earthquake sequence.

Introduction

Repeating earthquakes are characterized by highly correlated seismic waveforms, and are generally interpreted as reflecting repeated slip at small asperities on the same fault, surrounded by stably sliding regions on the plate boundary and active faults. In the past two decades, the cumulative seismic waveform data in the Seismic Analysis Code digital format, combined with a rapid increase in computational power and memory, have allowed easy identification of repeating earthquakes (or repeaters) based on high cross-correlation coefficients. The discovery of repeating earthquakes has led to increased interest in this research field. Repeaters can be used to monitor the spatial–temporal variations in quasi-static slip (rate) in subduction zones or along active faults (Nadeau and Johnson, 1998; Nadeau and McEvilly, 1999; Igarashi *et al.*, 2003; Uchida *et al.*, 2003, 2004; Uchida, Yui, *et al.*, 2009), and to estimate interplate coupling (Uchida, Nakajima, *et al.*, 2009; Igarashi, 2010; Uchida and Matsuzawa, 2011) and fault healing rates (Marone *et al.*, 1995; Peng *et al.*, 2005). The scaling relationship between recurrence time interval (T_r) and seismic moment (M_0) of repeaters can also be used to understand the parameters that influence the recurrence interval (T_r; Chen *et al.*, 2007). Repeating earthquakes with a regular T_r can be used as an assessment for understanding the long-term earthquake cycle model (Nadeau *et al.*, 1995; Matsuzawa *et al.*, 2002; Uchida *et al.*, 2007). In addition, earthquakes with highly correlated waveforms are extensively used to improve the precision of relative location among earthquake sequences and to map the details of sub-surface faults (Rubin *et al.*, 1999; Waldhauser and Ellsworth, 2000; Schaff *et al.*, 2002; Cheng *et al.*, 2007; Li *et al.*, 2007). Repeating earthquakes with identical locations, focal mechanisms, and moment rate functions, which can minimize the uncertainties due to earthquake source, are also used to detect subtle temporal changes in the seismic structure of the crust associated with large earthquakes (Poupinet *et al.*, 1984; Rubinstein and Beroza, 2004; Schaff and Beroza, 2004; Rubinstein and Beroza, 2005; Peng and Ben-Zion, 2006; Rubinstein *et al.*, 2007; Chao and Peng, 2009; Chen *et al.*, 2011) and Earth's deep interior (Zhang *et al.*, 2005; Wen, 2006; Zhang *et al.*, 2008).

Small repeating earthquakes with a periodic or a quasi-periodic recurrence interval, described as the continual-type

by Igarashi *et al.* (2003), were discovered on the Parkfield segment of the San Andreas fault (SAF; Nadeau *et al.*, 1995; Nadeau and Johnson, 1998; Nadeau and McEvilly, 1999), the Chihshang fault, and the Longitudinal Valley fault, Taiwan (Chen *et al.*, 2008, 2009), and in northeastern Japan (Igarashi *et al.*, 2003; Uchida *et al.*, 2007). Continual-type repeaters are located at small asperities surrounded by the stably sliding regions on the plate boundary. Burst-type repeaters (swarms or aftershocks) were also described by Igarashi *et al.* (2003), and are typically associated with large earthquakes, such as the 1984 Morgan Hill earthquake on the Calaveras fault, the 1989 Loma Prieta earthquake on the SAF (Vidale *et al.*, 1994; Schaff *et al.*, 1998; Schaff and Beroza, 2004; Peng *et al.*, 2005; Zhao and Peng, 2009), the 1999 Izmit and Düzce earthquakes on the North Anatolian fault in Turkey (Peng and Ben-Zion, 2006), and the 1994 far-off Sanriku and 2003 Tokachi-oki earthquakes in northeastern Japan (Igarashi *et al.*, 2003; Uchida, Yui, *et al.*, 2009). In subduction zones, burst-type repeaters are characterized by temporal clustering and can be located both down- and up-dip of the asperities of large earthquakes (i.e., the coseismic slip areas; Igarashi *et al.*, 2003; Uchida and Matsuzawa, 2011). Classification of continual- and burst-type is primarily based on differences in temporal behavior. The spatial distribution on the plate interface is essentially the same for both the continual- and burst-type repeaters (Igarashi *et al.*, 2003). However, moderate-sized (body-wave magnitude, $m_b > 4.7$) repeating earthquakes are less common, as the T_r would be long and follow the log–log $T_r - M_0$ scaling relationship (Nadeau and Johnson, 1998; Chen *et al.*, 2007). Moderate repeaters have been discovered on the Parkfield segment of the SAF (Nadeau and Johnson, 1998), several regions in circum-Pacific subduction zones (Zhang *et al.*, 2008), the South Sandwich islands (Zhang *et al.*, 2005), China (Schaff and Richards, 2004), Kamaishi-oki in northeastern Japan (Matsuzawa *et al.*, 2002; Uchida *et al.*, 2007), and at great depth inside the Tonga–Fiji slab (Wiens and Snider, 2001; Myhill *et al.*, 2011; Yu and Wen, 2012).

I am in the process of assembling teleseismic waveform data recorded by the Global Seismographic Network (GSN) and permanent regional seismic networks, and analyzing similar earthquake pairs for global subduction zones at all depth ranges. Previously, we searched for similar deep-focus earthquake pairs in the Tonga–Fiji subduction zone (Yu and Wen, 2012). Herein, a new dataset is analyzed comprising shallow-focus repeating earthquakes (focal depth < 70 km) along the Tonga–Kermadec and Vanuatu (former New Hebrides) subduction zones using teleseismic waveform data. A master-event algorithm (Wen, 2006) is used to determine the precise hypocentral relative locations and depths between earthquake pairs. I estimate the circular rupture zones assuming a Brune source model (Brune, 1970), and plot the estimated circular rupture zones relative to their precise locations. It is demonstrated that the majority of shallow correlated earthquake pairs are repeating earthquakes (i.e., earthquakes that have entirely overlapping rupture zones and comparable M_0). Finally, the $T_r - M_0$ scaling relationship is discussed, along with spatial–temporal variations in fault-slip rate, and interplate coupling in the Tonga–Kermadec–Vanuatu subduction zones.

Search for Repeating Earthquakes

Spatial separation and waveform cross correlation (cc) were used as the initial and secondary constraints to screen for potential earthquake pairs. Shallow events were first divided with $m_b > 4.7$ in the Preliminary Determination of Epicenters (PDE) catalog into a 0.5° by 0.5° grid in the Tonga–Kermadec–Vanuatu subduction zones (160° E–166° W, 6° S–42° S). An m_b magnitude threshold of 4.7 was adopted in order to have high signal-to-noise ratio (SNR) waveform records at teleseismic distances. I computed spatial separation between any two events within a grid element, and in the neighboring grid elements, for the entire study region. Events separated by < 80 km were considered as potential event pairs. A source separation of 80 km was used as the distance threshold to account for possible event mislocation in the PDE catalog. There are > 7900 shallow events with $m_b > 4.7$ in the database between 1990 and 2009, and more than 390,000 potential pairs satisfy the initial spatial separation constraint. I compiled seismic waveforms recorded by the GSN and regional seismic networks for each event (see Data and Resources; Fig. 1). I then band-pass filtered a 30-s time window after the direct *P* and *PKPdf* waves, which includes the *P*, *pP*, *sP*, *PKP*, *pPKP*, and *sPKP* phases in the frequency range of 0.8–2.0 Hz, and calculated the cc coefficient for all 390,000 potential pairs. The frequency range of 0.8–2.0 Hz can suppress the low-frequency background noise. More than 62 million waveform cc pairs were computed to search for similar earthquake pairs throughout the database. For the purpose of earthquake relocation, some pairs with < 5 cc measurements were excluded. I identified 128 correlated earthquake pairs with an average cc coefficient of > 0.8 computed from > 5 measurements.

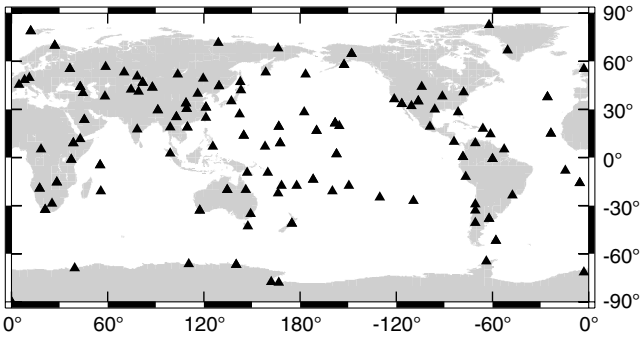

Figure 1. Map of the seismic stations used to search for correlated earthquake pairs. Seismic stations belong to the Global Seismographic Network (GSN), the Global Telemetered Seismograph Network (GT), GEOSCOPE (G), and the new China Digital Seismograph Network (CD, IC). Note that the status of the network is as of December 2001, and these seismic networks have progressively expanded since that time.

Among these correlated event pairs, some pairs that share an event in common were further grouped as clusters (comprising 3–5 events), whereas others comprising just two events were referred to as doublets.

A total of 22 clusters and 31 doublets were identified along the Tonga–Kermadec–Vanuatu subduction zones (Fig. 2, Tables 1 and 2). These correlated earthquake pairs occurred at the plate interface with low-angle thrust-fault focal mechanisms (Fig. 2). Along the Tonga plate-interface region, the majority of the correlated event pairs are spatially clustered between 19° S and 21.5° S (T1 and T2 regions in Fig. 2a), where the plate convergence rate is inferred from the Global Positioning System (GPS) data to be 16.4–20.5 cm/yr (Bevis *et al.*, 1995; Fig. 3, Table 3). Along the Kermadec and Vanuatu plate-interface regions, the spatial distribution of the correlated pairs is sporadic (Fig. 2). There are more clusters and doublets along the Tonga interplate region than along the Kermadec and Vanuatu interplate regions (Fig. 2). The majority of the interplate clusters and doublets are continual-type with a time separation on the order of years (Fig. 4). The burst-type correlated event pairs with short time separations of months to a year are the TS-D2, KS-D19, KS-D27, and VS-D1 doublets, and the 2007/08/23 and 2007/09/05 events of the VS-C2 cluster, the 2008/04/06 and 2008/06/01 events of the VS-C4 cluster, and the NFS-C9 cluster (Fig. 4). Several burst-type correlated clusters and doublets appear to be associated with large interplate earthquakes. The TS-D2 doublet may be associated with the 2009/09/29 Samoa–Tonga outer trench-slope earthquake (M_w 8.1) that triggered large interplate doublets (both of M_w 7.8; Lay *et al.*, 2010; Figs. 2a and 3). Near 165.7° E, 11.4° S in the northern Vanuatu interplate region, the 2007/09/02 earthquake (M_w 7.3) and the 2009/10/07 earthquake triplet (M_w 7.7, M_w 7.8, and M_w 7.4) likely induced the 2007/09/05 and 2009/10/08 events of the VS-C2 cluster and the 2009/10/15 event of the VS-D1 doublet (Figs. 2b, 3, and 4). In the V3 interplate region in Vanuatu, the 2008/04/09 M_w 7.3 earthquake and associated aseismic slip probably induced the 2008/04/10 event of the VS-C6 cluster and the 2008/06/01 event of the VS-C4 cluster (Figs. 2b, 3, and 4). The NFS-C9 cluster that occurred in the North Fiji basin is distinct from the interplate clusters and doublets, and is characterized by temporal clustering during November 1997 and normal-fault focal mechanisms (Figs. 2b and 4b, Table 1).

These shallow similar earthquake pairs exhibit highly correlated waveforms. Figure 5 displays examples of high-frequency *P*- and *S*-wave coda waveforms in a 45-s time window for the clusters TS-C3 and VS-C5 at regional and teleseismic distances. For the TS-C3 cluster, the waveform cc coefficient can approach 0.9 for the *P*-wave coda and 0.95 for the *S*-wave coda recorded at the closest station AFI (Fig. 5a). The cc coefficient of the *P*-wave coda can approach 0.9 and above for the records with high SNR (Fig. 5b–f). For the VS-C5 cluster, the cc coefficient can reach 0.95 and above for the available *P* and *S* coda recorded by the closest stations DZM and NOUC (Fig. 5g,i). The cc coefficient of the *P*-wave coda can often approach 0.95 at teleseismic distances (Fig. 5h,j, and k).

Master-Event Algorithm

I use a master-event algorithm (Wen, 2006) to determine the precise relative location and depth between shallow-event pairs. This algorithm treats one event of the pair as the master (or reference) event for which the origin time and hypocenter are fixed to those of the PDE catalog. The error on the origin time and relative location and depth of the second event are solved via a grid searching technique. The data are the travel-time residuals of the seismic-phase pairs calculated by waveform cc of the high-frequency waveform pairs. The *P*, *pP*, and *PKP* phase pairs are included in the master-event relocation algorithm. Surface-reflected *pP* phases sampling the upper focal hemisphere are used to improve the precision on the relative depth estimates. The travel-time residual is sensitive to differential location and depth, and origin-time error between two earthquakes, and is insensitive to heterogeneous velocity structures along the ray paths because the event pair should have nearly identical ray paths. Whereas the absolute location and depth of the master event might be biased by the 3D heterogeneous velocity structures near source, the relative location between earthquake pairs should still be precise. Event-origin time error is treated as a constant and is calculated by averaging the travel-time residuals for a given earthquake pair. The optimum location and depth of the second event relative to the master event are solved by grid searching the region near the master event that yields the minimum root-mean-square (rms) time residual. The box for the grid search is 12 km (east–west) by 12 km (north–south) by 12 km (vertical) centered on the hypocenter of the master event. The interval used for the grid search is 100 m. To achieve sub-sample precision, the time series are interpolated to 5-milliseconds (ms) sampling rate before cc.

To estimate the location uncertainties, I compute the 95%-confidence ellipse for each event pair with 200 bootstrap re-samplings. Eighty percent of the travel-time residuals of the seismic phases are randomly selected and used in each bootstrap calculation. The 95%-confidence ellipse is estimated using a least squares fit to the 200 locations. Precision of the location uncertainties depends on the geometry of seismograph distribution, the epicentral distance that influences the sensitivity of horizontal slowness, and the number of measurements. With adequate azimuthal coverage, bootstrap re-samplings can constrain the reliability of the location uncertainties (Waldhauser and Ellsworth, 2000).

Relocation Results and Identification of Repeating Earthquakes

One relocation exercise for the TS-C3-99r-94 event pair, consisting of events 1999/06/21 (m_b 5.0, 33-km depth, labeled as 99r) and 1994/05/15 (m_b 5.2, 33.2-km depth, labeled as 94) is displayed in Figure 6 as an example. The TS-C3-99r-94 pair has reasonably good sampling

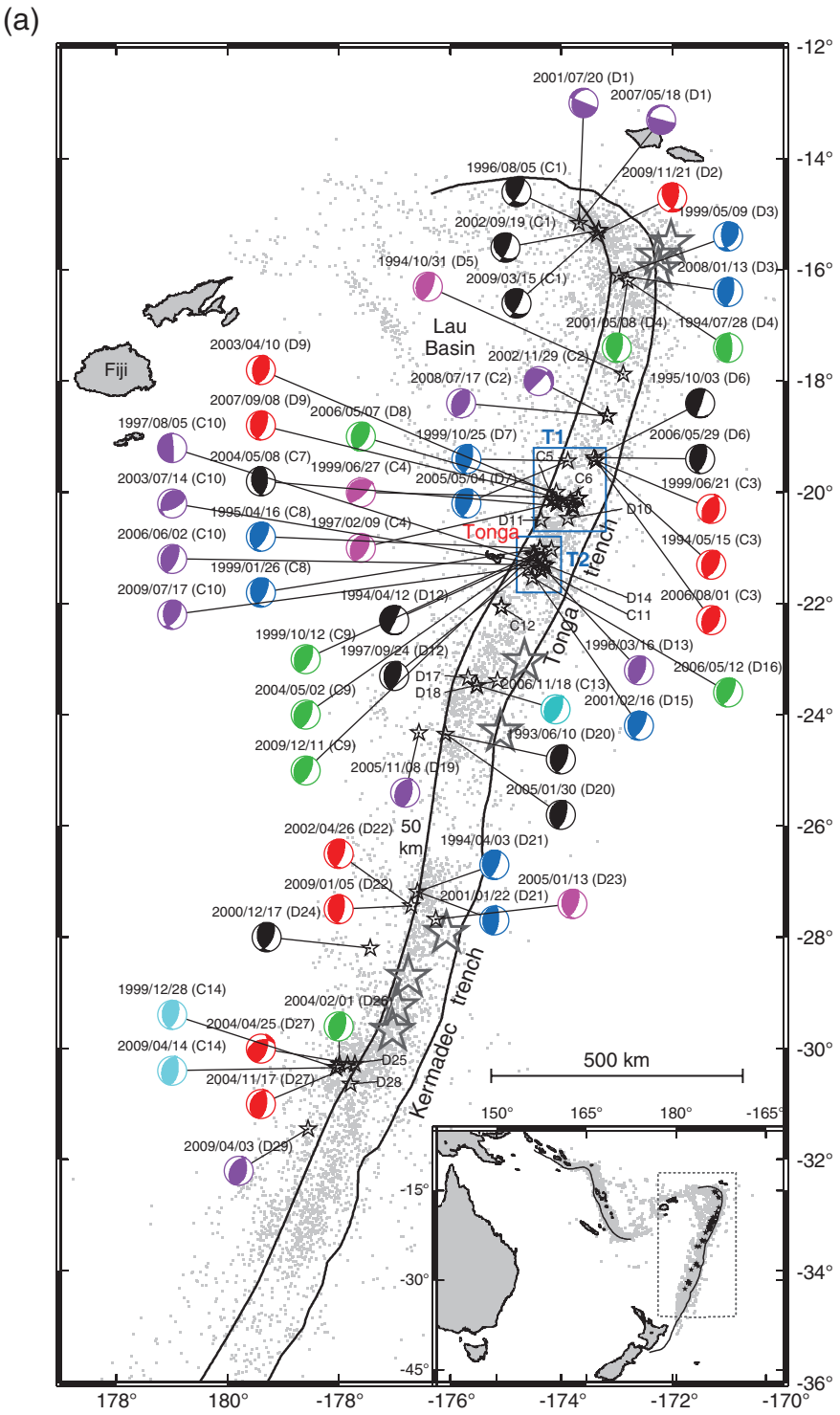

Figure 2. Regional map of moderate-sized ($m_b > 4.7$) shallow-focus repeating earthquakes and background seismicity along the (a) Tonga–Kermadec and (b) Vanuatu (former New Hebrides) subduction zones. Shallow repeating earthquakes (black stars) and their available Global Centroid Moment Tensor (GCMT; Dziewoński *et al.*, 1981; Ekström *et al.*, 2003) are labeled with event date and doublet/cluster id where applicable. Colors of GCMT are used to distinguish nearby different repeaters. Source parameters for the clusters and doublets are listed in Tables 1 and 2. Background seismicity is shown as gray dots and large interplate earthquakes (moment magnitude, $M_w > 7.3$) since 1976 are shown as large open gray stars. Black lines indicate the trench (Bird, 2003) and slab contour at 50-km depth (Gudmundsson and Sambridge, 1998). Repeating earthquake clusters in the (a) T1 and T2 plate-interface regions in Tonga and (b) V3 plate-interface region in Vanuatu are used to study the fault-slip rate ($\dot{d}$). A regional map of the Tonga–Kermadec–Vanuatu subduction zones is shown in the inset figure, with the gray dotted box indicating the expanded region in the main figure. (*Continued*)

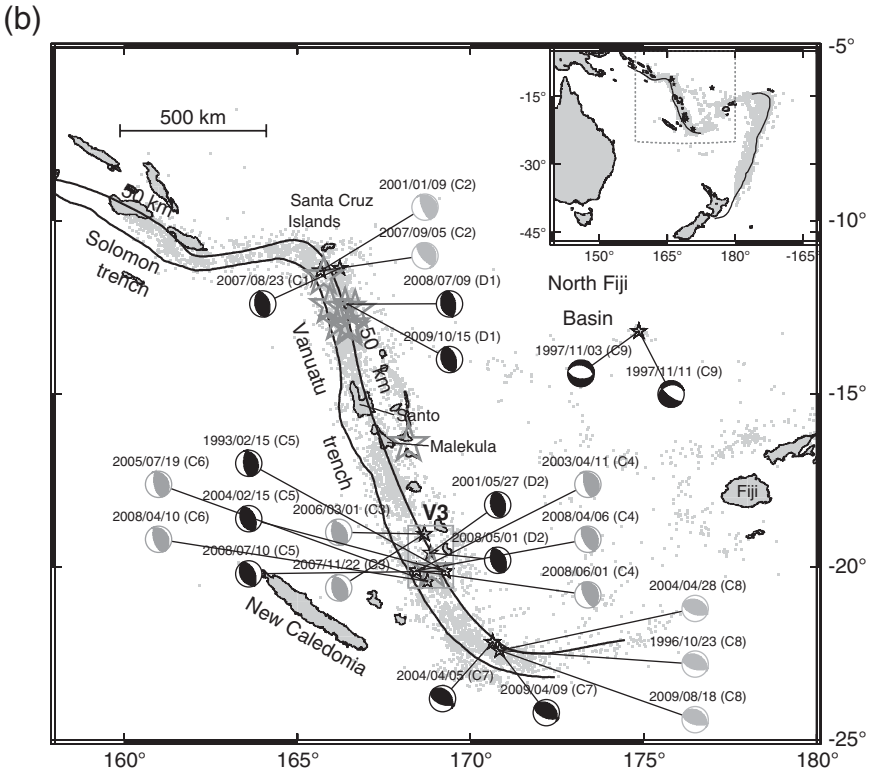

Figure 2. Continued.

coverage at regional and teleseismic distances (Fig. 6a,b). The master-event relocation shows that the TS-C3-99r-94 pair is separated by 0.15 and 0.2 km in the horizontal and vertical planes, respectively (Fig. 6c). The major and minor axes of the 95% confidence ellipse of the location uncertainties in the horizontal plane are 0.58 and 0.30 km, respectively (white ellipse in Fig. 6c, Table 1). The travel-time residuals are within ±30 ms (Fig. 6b), and the rms time residual predicted on the basis of optimum location and depth of the second event is 13 ms (Fig. 6c, Table 1). The cc coefficient of most high-frequency *P* and surface-reflected *pP* and *sP* waveforms with high SNR in the distance range of 30° to 100° can also approach 0.85 and above (Fig. 6d,e).

Overall, the master-event relocation results suggest that most clusters and doublets are separated by hundreds of meters in the horizontal and vertical planes, except for a few cases that are offset by > 1 km. The master-event algorithm can greatly improve the precision of relative locations and depths from the PDE catalog with, for example, location uncertainties in the horizontal plane often being less than a few kilometers (Tables 1 and 2).

It is essential to estimate the rupture areas of individual earthquakes and plot rupture areas relative to the precise location of the hypocenters, in order to determine whether the rupture areas overlap among these earthquake pairs. I first relate magnitude (m_b) to scalar seismic moment (M_0; dyn·cm; Hanks and Kanamori, 1979). The radius of earthquake rupture zones is estimated based on the relationship:

$$M_0 = (16/7)\Delta\sigma a^3, \quad (1)$$

for which $\Delta\sigma$ is the stress drop and a is the radius of a circular fault. I use a stress drop of 1 MPa for interplate earthquakes (Kanamori and Anderson, 1975). The estimated circular rupture zone for moderate interplate earthquakes is 2–5 km.

Figures 7 and 8 display the estimated earthquake rupture zones relative to the precise location of these correlated clusters and doublets. Their spatial separation is usually much smaller than the estimated circular source areas. Thus, these clusters and doublets have entirely overlapping source areas. Moreover, the majority of these earthquakes have similar circular source areas or M_0. Both of these observations imply that the majority of these earthquakes re-rupture over the same fault area and can be defined as repeating earthquakes. Note that several similar earthquake pairs do not satisfy the definition of repeating earthquakes in that these pairs are offset by 1–2 km in the horizontal and vertical planes, or their source areas are not entirely overlapped, and/or do not have similar M_0. The similar earthquake pairs are the TS-C1, KS-C14, NFS-C9 clusters, the 2001/07/04 (m_b 4.8) and 2007/12/04 (m_b 4.8) events of the VS-C7 cluster, and the TS-D2, TS-D12, and KS-D27 doublets (Figs. 7 and 8, Tables 1 and 2). My analyses suggest that cross correlation can be used as a preliminary index to identify similar earthquake pairs and repeaters. Apart from having a high cc coefficient, repeating earthquakes can be better defined as the correlated earthquake pairs that have entirely overlapping source areas and similar M_0.

Table 1

Shallow-Focus Clusters along the Tonga–Kermadec–Vanuatu Subduction Zones

Origin Date (yyyy/mm/dd)	Origin Time (hh:mm:ss.ss)	Latitude (°N)	Longitude (°E)	Depth (km)	m_b	dt (yr)	cc	N_{ph}	rms (ms)	dh_c (km)	dz_c (km)	dh_r (km)	dz_r (km)	$ellp_{maj}$ (km)	$ellp_{min}$ (km)
TS-C1															
1996/08/05	17:01:05.20	−15.293	−173.332	33.0	4.9	—	1.00	—	—	—	—	—	—	—	—
2002/09/19	10:15:03.67	−15.289	−173.342	34.0	4.9	6.1	0.84	18	32	10.90	0.00	1.16	1.00	1.23	0.89
2009/03/15	20:28:54.52	−15.292	−173.334	32.9	5.5	12.6	0.80	13	24	18.34	2.00	0.24	−0.10	0.78	0.34
TS-C2															
1996/10/12	11:48:24.91	−18.629	−173.171	33.0	4.7	—	1.00	—	—	—	—	—	—	—	—
2002/11/29	05:49:41.03	−18.628	−173.170	33.0	4.9	6.1	0.85	19	15	21.21	0.00	0.15	0.00	0.86	0.59
2008/07/17	09:48:44.81	−18.629	−173.172	33.3	4.9	11.8	0.87	14	12	27.18	−11.50	0.11	0.30	1.11	0.78
TS-C3															
1999/06/21	13:09:41.80	−19.425	−173.381	33.0	5.0	—	1.00	—	—	—	—	—	—	—	—
1994/05/15	13:46:34.18	−19.424	−173.380	33.2	5.2	−5.1	0.90	28	13	49.77	−10.00	0.15	0.20	0.58	0.30
2006/08/01	10:19:43.20	−19.426	−173.379	33.2	5.2	7.1	0.89	30	15	33.57	−2.00	0.24	0.20	0.43	0.29
TS-C4															
1999/06/27	14:01:39.10	−20.105	−173.692	33.0	4.9	—	1.00	—	—	—	—	—	—	—	—
1995/05/08	12:06:38.79	−20.105	−173.693	32.8	4.9	−4.1	0.90	17	11	16.20	0.00	0.10	−0.20	0.43	0.21
1997/02/09	23:11:05.15	−20.106	−173.692	33.0	5.0	−2.4	0.90	23	8	15.88	7.00	0.11	0.00	1.09	0.67
2001/04/04	10:53:24.97	−20.105	−173.692	32.9	4.7	1.8	0.87	28	12	7.82	0.00	0.00	−0.10	0.56	0.44
2002/05/10	10:59:50.85	−20.106	−173.693	33.3	5.0	2.9	0.83	21	20	10.94	0.00	0.15	0.30	2.01	0.71
TS-C5															
1996/10/05	10:51:11.05	−20.126	−174.154	33.0	4.7	—	1.00	—	—	—	—	—	—	—	—
1999/07/20	05:53:43.50	−20.126	−174.153	33.0	4.8	2.8	0.88	14	12	39.14	0.00	0.10	0.00	1.11	0.44
2003/10/09	16:02:52.47	−20.125	−174.154	33.0	5.0	7.0	0.88	9	12	7.52	0.00	0.11	0.00	16.29	13.92
2005/09/15	20:06:59.15	−20.131	−174.153	32.9	4.8	8.9	0.86	12	17	2.46	−23.00	0.57	−0.10	2.25	1.01
2006/05/27	19:40:33.66	−20.130	−174.152	32.9	4.9	9.6	0.85	10	10	17.62	2.00	0.49	−0.10	15.07	8.78
TS-C6															
1996/09/11	13:25:54.00	−20.198	−174.080	33.0	4.7	—	1.00	—	—	—	—	—	—	—	—
2002/02/15	14:04:09.24	−20.198	−174.083	33.1	4.8	5.4	0.80	12	8	28.27	0.00	0.31	0.10	1.36	1.00
2004/06/12	15:09:37.23	−20.198	−174.084	33.2	4.7	7.8	0.82	14	13	9.45	−18.00	0.42	0.20	1.33	0.58
2006/03/30	12:19:48.49	−20.197	−174.084	32.8	4.8	9.5	0.83	8	9	8.56	1.00	0.43	−0.20	1.23	1.05
TS-C7															
2004/05/08	23:03:38.22	−20.267	−173.791	35.0	4.9	—	1.00	—	—	—	—	—	—	—	—
1993/12/14	06:47:43.07	−20.273	−173.792	35.6	5.2	−10.4	0.84	17	18	64.84	2.00	0.67	0.60	5.46	1.01
1999/08/21	06:25:35.50	−20.268	−173.791	34.7	4.9	−4.7	0.88	21	10	20.43	−2.00	0.11	−0.30	0.46	0.27
TS-C8															
1995/04/16	20:36:09.00	−21.017	−174.386	32.0	5.0	—	1.00	—	—	—	—	—	—	—	—
1991/09/07	22:07:41.23	−21.020	−174.389	32.2	5.2	−3.6	0.92	14	10	16.53	27.00	0.46	0.20	3.97	1.52
1999/01/26	07:04:20.25	−21.017	−174.386	31.8	4.9	3.8	0.88	21	20	13.89	1.00	0.00	−0.20	1.03	0.74
TS-C9															
1999/10/12	13:27:45.60	−21.116	−174.489	33.0	5.4	—	1.00	—	—	—	—	—	—	—	—
2004/05/02	05:11:19.42	−21.114	−174.491	32.9	5.5	4.6	0.85	50	13	8.05	−23.00	0.30	−0.10	1.33	0.67
2009/12/11	12:33:37.23	−21.116	−174.491	32.7	5.6	10.2	0.89	39	15	7.91	−23.00	0.21	−0.30	0.48	0.23

(*continued*)

Table 1 (*Continued*)

Origin Date (yyyy/mm/dd)	Origin Time (hh:mm:ss.ss)	Latitude (°N)	Longitude (°E)	Depth (km)	m_b	dt (yr)	cc	N_{ph}	rms (ms)	dh_c (km)	dz_c (km)	dh_r (km)	dz_r (km)	$ellp_{maj}$ (km)	$ellp_{min}$ (km)
TS-C10															
1997/08/05	20:45:27.20	−21.310	−174.288	33.0	4.9	—	1.00	—	—	—	—	—	—	—	—
1999/11/30	04:40:25.27	−21.309	−174.287	32.9	5.1	2.3	0.88	23	19	14.39	0.00	0.15	−0.10	2.74	1.15
2003/07/14	18:19:42.36	−21.307	−174.291	32.6	4.8	5.9	0.85	29	21	6.48	0.00	0.46	−0.40	1.59	0.86
2006/06/02	03:26:44.10	−21.310	−174.288	32.6	5.0	8.8	0.87	23	11	8.62	4.00	0.00	−0.40	1.70	0.70
2009/07/17	00:59:54.91	−21.310	−174.286	33.2	5.0	11.9	0.88	18	11	9.12	20.30	0.21	0.20	0.71	0.49
TS-C11															
1999/02/12	13:47:50.00	−21.398	−174.370	33.0	5.1	—	1.00	—	—	—	—	—	—	—	—
1995/08/14	21:06:21.25	−21.397	−174.373	32.5	4.7	−3.5	0.83	22	20	41.99	0.00	0.33	−0.50	2.33	0.96
2004/05/24	22:41:15.28	−21.397	−174.370	33.1	4.8	5.3	0.83	16	14	42.02	42.00	0.11	0.10	1.40	0.85
2007/03/13	00:14:29.21	−21.398	−174.372	32.4	4.9	8.1	0.85	23	13	24.82	2.00	0.21	−0.60	0.95	0.46
TS-C12															
2000/02/08	00:42:27.23	−22.066	−175.078	33.0	4.8	—	1.00	—	—	—	—	—	—	—	—
1996/04/22	06:09:18.15	−22.065	−175.076	33.1	4.7	−3.8	0.86	7	7	11.71	0.00	0.23	0.10	16.79	8.61
2008/03/14	15:48:32.90	−22.068	−175.080	32.6	5.0	8.1	0.90	11	5	43.94	2.00	0.30	−0.40	4.34	1.46
TS-C13															
2002/06/20	05:26:10.64	−23.473	−175.518	33.0	5.1	—	1.00	—	—	—	—	—	—	—	—
1997/03/12	01:55:00.71	−23.473	−175.514	32.8	5.0	−5.3	0.85	10	10	2.47	0.00	0.41	−0.20	6.08	3.41
2006/11/18	21:45:13.95	−23.474	−175.516	33.2	5.0	4.4	0.83	23	15	3.83	9.00	0.23	0.20	0.51	0.34
KS-C14															
1999/12/28	19:15:36.90	−30.353	−178.051	33.0	5.0	—	1.00	—	—	—	—	—	—	—	—
1993/05/19	11:55:44.27	−30.352	−178.046	32.8	5.5	−6.6	0.80	11	19	15.21	−10.00	0.49	−0.20	1.99	1.33
2009/04/14	12:49:03.31	−30.353	−178.043	31.4	5.2	9.3	0.80	16	19	16.84	14.50	0.77	−1.60	1.87	1.01
VS-C1															
2001/08/19	05:57:51.75	−11.366	166.228	50.0	4.8	—	1.00	—	—	—	—	—	—	—	—
1995/11/20	20:48:05.11	−11.367	166.229	49.9	4.7	−5.7	0.81	9	9	16.95	−17.00	0.16	−0.10	1.21	0.50
2007/08/23	07:04:22.36	−11.366	166.226	50.2	4.9	6.0	0.86	13	8	4.75	18.00	0.22	0.20	0.61	0.27
VS-C2															
2001/01/09	12:53:15.52	−11.446	165.670	33.0	4.9	—	1.00	—	—	—	—	—	—	—	—
2007/08/23	23:36:42.59	−11.447	165.668	32.9	4.9	6.6	0.88	14	15	4.42	41.00	0.24	−0.10	1.11	0.67
2007/09/05	14:22:19.02	−11.447	165.668	32.6	4.9	6.7	0.82	14	16	12.22	2.00	0.24	−0.40	1.56	1.11
2009/10/08	06:07:12.69	−11.448	165.668	33.3	5.0	8.7	0.86	11	9	5.22	2.00	0.31	0.30	1.11	0.61
VS-C3															
2001/03/13	14:41:35.04	−19.047	168.668	33.0	4.7	—	1.00	—	—	—	—	—	—	—	—
2006/03/01	19:00:53.04	−19.047	168.666	33.2	4.9	5.0	0.88	16	7	8.67	5.00	0.21	0.20	0.97	0.52
2007/11/22	20:30:22.98	−19.046	168.669	32.5	5.0	6.7	0.85	21	10	15.33	7.00	0.15	−0.50	0.50	0.44
VS-C4															
1999/04/08	16:03:06.20	−20.103	168.442	33.0	4.8	—	1.00	—	—	—	—	—	—	—	—
2003/04/11	17:57:15.33	−20.101	168.444	33.5	4.9	4.0	0.85	14	16	21.23	0.00	0.30	0.50	2.03	1.33
2008/04/06	18:48:15.47	−20.101	168.441	33.2	5.1	9.0	0.88	15	19	14.10	2.00	0.25	0.20	1.28	0.78
2008/06/01	22:30:51.86	−20.102	168.445	32.7	5.1	9.2	0.91	13	20	17.22	12.50	0.33	−0.30	1.89	1.22

(*continued*)

Table 1 (*Continued*)

Origin Date (yyyy/mm/dd)	Origin Time (hh:mm:ss.ss)	Latitude (°N)	Longitude (°E)	Depth (km)	m_b	dt (yr)	cc	N_{ph}	rms (ms)	dh_c (km)	dz_c (km)	dh_r (km)	dz_r (km)	$ellp_{maj}$ (km)	$ellp_{min}$ (km)
VS-C5															
1998/05/14	20:03:17.60	−20.119	169.276	49.0	5.2	—	1.00	—	—	—	—	—	—	—	—
1993/02/15	12:02:14.16	−20.123	169.273	49.2	5.1	−5.2	0.92	14	9	12.79	−3.00	0.54	0.20	1.56	1.11
2004/02/15	00:01:32.04	−20.120	169.275	48.7	5.3	5.8	0.94	34	10	10.90	−3.00	0.15	−0.30	0.31	0.26
2008/07/10	16:01:09.12	−20.118	169.276	48.0	5.2	10.2	0.92	28	12	8.53	20.50	0.11	−1.00	0.52	0.34
VS-C6															
1999/04/19	09:38:38.70	−20.416	168.766	33.0	4.8	—	1.00	—	—	—	—	—	—	—	—
2005/07/19	14:55:08.18	−20.413	168.766	32.9	4.9	6.2	0.87	15	23	23.61	8.00	0.33	−0.10	1.27	0.92
2008/04/10	13:25:30.02	−20.414	168.766	32.9	4.8	9.0	0.89	15	22	15.92	2.00	0.22	−0.10	0.92	0.64
VS-C7															
2004/04/05	18:40:03.77	−22.162	170.645	10.0	5.3	—	1.00	—	—	—	—	—	—	—	—
2001/07/04	16:58:04.38	−22.163	170.640	9.3	4.8	−2.8	0.86	15	8	14.08	23.00	0.53	−0.70	3.16	1.33
2007/12/04	20:34:48.47	−22.170	170.642	8.9	4.8	3.7	0.87	22	7	26.91	7.00	0.94	−1.10	1.45	0.89
2009/04/09	04:13:12.63	−22.162	170.646	9.4	5.4	5.0	0.90	33	8	1.78	25.00	0.10	−0.60	0.56	0.32
VS-C8															
2004/04/28	09:53:02.62	−22.402	170.843	10.0	5.0	—	1.00	—	—	—	—	—	—	—	—
1996/10/23	10:18:57.15	−22.399	170.841	10.3	4.9	−7.5	0.83	18	10	13.64	23.00	0.39	0.30	0.52	0.40
2009/08/18	00:59:50.01	−22.400	170.842	10.2	5.0	5.3	0.91	18	7	14.15	45.00	0.24	0.20	0.63	0.43
NFS-C9															
1997/11/11	02:00:36.50	−13.192	174.864	11.0	5.3	—	1.00	—	—	—	—	—	—	—	—
1997/11/03	06:29:16.53	−13.189	174.869	8.9	5.2	0.0	0.82	8	15	2.30	0.00	0.64	−2.10	1.11	0.60
1997/11/06	21:43:54.68	−13.190	174.869	10.0	5.3	0.0	0.76	23	24	1.72	0.00	0.58	−1.00	1.47	0.82
1997/11/07	09:25:12.80	−13.196	174.862	13.5	4.8	0.0	0.80	8	15	7.73	0.00	0.49	2.50	11.25	3.77
1997/11/12	19:33:45.34	−13.187	174.862	11.5	4.8	0.0	0.86	14	16	6.63	0.00	0.60	0.50	0.74	0.22

The first event of each cluster refers to the reference (master) event with the origin time of the reference event fixed to that of the PDE catalog. The event-origin time of the second event is corrected for the origin-time error within the cluster as inferred from the master-event algorithm. m_b is body-wave magnitude; dt is the time separation between the reference and second events in years (yr); cc is the average cross-correlation coefficient calculated by the number of seismic phases (N_{ph}) used for the master-event relocation; rms is the root-mean-square time residual within the cluster predicted based on the optimum location and depth of the second event relative to the reference event in milliseconds (ms); dh_c and dz_c are the horizontal and vertical separations within the cluster based on the PDE catalog; dh_r and dz_r are the horizontal and vertical separations within the cluster inferred from the master-event relocation; $ellp_{maj}$ and $ellp_{min}$ are the major and minor axes of the 95% confidence ellipse in the horizontal plane.

Table 2
Shallow-Focus Doublets along the Tonga–Kermadec–Vanuatu Subduction Zones

Origin Date (yyyy/mm/dd)	Origin Time (hh:mm:ss.ss)	Latitude (°N)	Longitude (°E)	Depth (km)	m_b	dt (yr)	cc	N_{ph}	rms (ms)	dh_c (km)	dz_c (km)	dh_r (km)	dz_r (km)	$ellp_{maj}$ (km)	$ellp_{min}$ (km)
TS-D1															
2001/07/20	00:21:51.47	−15.167	−173.687	40.0	5.2	—	1.00	—	—	—	—	—	—	—	—
2007/05/18	09:49:04.80	−15.166	−173.690	39.4	5.2	5.8	0.83	31	30	17.31	1.00	0.34	–0.60	0.92	0.56
TS-D2															
2009/09/29	22:08:30.00	−15.375	−173.359	10.0	5.1	—	1.00	—	—	—	—	—	—	—	—
2009/11/21	19:30:32.17	−15.377	−173.365	11.0	5.0	0.1	0.82	33	13	8.56	26.20	0.68	1.00	0.63	0.31
TS-D3															
1999/05/09	00:35:02.90	−16.102	−172.961	33.0	4.8	—	1.00								
2008/01/13	11:16:42.38	−16.099	−172.961	32.9	5.1	8.7	0.85	22	18	5.62	3.60	0.33	−0.10	1.05	0.69
TS-D4															
1994/07/28	01:39:07.10	−16.194	−172.806	33.0	4.9	—	1.00	—	—	—	—	—	—	—	—
2001/05/08	16:40:34.57	−16.198	−172.808	33.2	4.9	6.8	0.84	12	17	24.45	0.00	0.49	0.20	2.49	1.16
TS-D5															
1994/10/31	23:04:08.60	−17.876	−172.883	33.0	5.2	—	1.00	—	—	—	—	—	—	—	—
2000/10/04	15:39:27.08	−17.875	−172.884	32.6	5.1	5.9	0.88	11	24	36.40	0.00	0.15	−0.40	4.15	1.81
TS-D6															
1995/10/03	18:38:30.70	−19.381	−173.416	33.0	5.2	—	1.00	—	—	—	—	—	—	—	—
2006/05/29	11:56:46.80	−19.382	−173.416	32.7	5.2	10.7	0.87	20	15	21.69	0.00	0.11	−0.30	0.73	0.49
TS-D7															
1999/10/25	00:01:20.50	−19.442	−173.880	33.0	5.5	—	1.00	—	—	—	—	—	—	—	—
2005/05/04	08:57:01.05	−19.442	−173.880	33.0	5.7	5.5	0.88	61	16	6.61	−11.00	0.00	0.00	0.29	0.18
TS-D8															
2000/09/10	23:09:08.37	−20.003	−174.093	33.0	4.8	—	1.00	—	—	—	—	—	—	—	—
2006/05/07	22:06:29.81	−20.003	−174.092	33.6	4.9	5.7	0.87	22	12	28.57	2.00	0.10	0.60	0.89	0.36
TS-D9															
2003/04/10	15:11:47.92	−20.244	−173.798	33.0	5.1	—	1.00	—	—	—	—	—	—	—	—
2007/09/08	03:14:53.54	−20.245	−173.799	32.9	5.1	4.4	0.86	28	9	10.59	2.00	0.15	−0.10	0.32	0.14
TS-D10															
1993/12/16	04:18:19.20	−20.473	−173.884	24.0	5.1	—	1.00	—	—	—	—	—	—	—	—
2001/04/22	07:48:56.07	–20.468	–173.884	23.8	4.9	7.3	0.80	11	15	23.17	9.00	0.56	–0.20	10.15	5.82
TS-D11															
2000/11/24	17:27:11.16	−20.508	−174.367	35.0	5.3	—	1.00	—	—	—	—	—	—	—	—
2004/05/22	07:36:57.90	−20.508	−174.367	35.0	5.2	3.5	0.95	14	5	11.87	−2.00	0.00	0.00	0.51	0.24
TS-D12															
1994/04/12	14:42:49.90	−21.034	−174.175	31.0	5.1	—	—	—	—	—	—	—	—	—	—
1997/09/24	15:16:27.96	−21.028	−174.178	30.2	4.9	3.5	0.87	11	16	10.23	2.00	0.74	−0.80	4.05	2.76
TS-D13															
1996/03/16	11:49:43.60	−21.150	−174.510	33.0	4.9	—	1.00	—	—	—	—	—	—	—	—
2002/08/04	17:25:07.62	−21.148	−174.513	33.6	4.7	6.4	0.88	13	13	18.28	0.00	0.38	0.60	3.38	1.48
TS-D14															
1997/10/26	22:10:11.10	−21.280	−174.337	33.0	4.9	—	1.00	—	—	—	—	—	—	—	—
2002/05/31	18:28:52.17	−21.281	−174.339	32.4	5.2	4.6	0.86	16	15	17.04	0.00	0.23	−0.60	1.36	0.83

(*continued*)

Table 2 (*Continued*)

Origin Date (yyyy/mm/dd)	Origin Time (hh:mm:ss.ss)	Latitude (°N)	Longitude (°E)	Depth (km)	m_b	dt (yr)	cc	N_{ph}	rms (ms)	dh_c (km)	dz_c (km)	dh_r (km)	dz_r (km)	$ellp_{maj}$ (km)	$ellp_{min}$ (km)
TS-D15															
2001/02/16	17:44:35.35	−21.369	−174.591	33.0	5.1	—	1.00	—	—	—	—	—	—	—	—
2007/04/16	15:50:04.91	−21.372	−174.589	32.9	5.2	6.2	0.84	31	13	10.23	−23.00	0.39	−0.10	0.33	0.24
TS-D16															
2001/02/16	16:29:16.45	−21.537	−174.522	33.0	4.9	—	1.00	—	—	—	—	—	—	—	—
2006/05/12	21:52:47.82	−21.539	−174.521	32.5	5.0	5.2	0.84	24	9	19.14	17.00	0.25	−0.50	0.30	0.16
TS-D17															
2003/12/10	17:19:43.48	−23.336	−175.678	33.0	4.9	—	1.00	—	—	—	—	—	—	—	—
2006/11/11	17:34:00.00	−23.336	−175.677	33.0	4.8	2.9	0.82	12	16	10.57	−23.00	0.10	0.00	1.12	0.78
TS-D18															
2000/05/21	21:53:32.73	−23.393	−175.144	33.0	4.7	—	1.00	—	—	—	—	—	—	—	—
2008/07/21	20:14:52.63	−23.394	−175.150	33.5	4.8	8.2	0.89	19	13	26.37	32.90	0.62	0.50	0.74	0.34
KS-D19															
2004/11/05	19:34:19.70	−24.330	−176.561	44.0	4.7	—	1.00	—	—	—	—	—	—	—	—
2005/11/08	02:56:16.28	−24.330	−176.558	43.7	5.0	1.0	0.80	26	14	3.22	−10.00	0.30	−0.30	1.11	0.78
KS-D20															
1993/06/10	17:48:38.30	−24.353	−176.082	34.0	5.7	—	1.00	—	—	—	—	—	—	—	—
2005/01/30	08:08:27.65	−24.350	−176.082	34.0	5.5	11.6	0.93	17	14	11.61	−2.00	0.33	0.00	2.80	1.16
KS-D21															
1994/04/03	12:56:43.60	−27.185	−176.583	34.0	5.2	—	1.00	—	—	—	—	—	—	—	—
2001/01/22	02:31:07.84	−27.186	−176.583	33.7	5.1	6.8	0.87	10	16	3.49	−1.00	0.11	−0.30	4.75	2.20
KS-D22															
2002/04/26	02:12:56.64	−27.441	−176.702	33.0	5.3	—	1.00	—	—	—	—	—	—	—	—
2009/01/05	22:27:15.12	−27.441	−176.702	33.0	5.2	6.7	0.93	30	8	4.35	14.00	0.00	0.00	0.21	0.16
KS-D23															
1993/11/24	05:49:52.10	−27.677	−176.257	33.0	5.3	—	1.00	—	—	—	—	—	—	—	—
2005/01/13	17:14:04.24	−27.675	−176.257	33.2	5.2	11.1	0.91	7	8	73.02	−23.00	0.22	0.20	9.51	4.69
KS-D24															
1993/09/15	05:40:57.80	−28.198	−177.440	61.0	5.4	—	1.00	—	—	—	—	—	—	—	—
2000/12/17	02:29:14.48	−28.204	−177.438	60.6	5.0	7.3	0.87	11	11	0.83	13.00	0.69	−0.40	1.90	1.39
KS-D25															
2003/06/04	06:03:43.53	−30.286	−177.842	33.0	5.0	—	1.00	—	—	—	—	—	—	—	—
2007/08/14	05:52:35.65	−30.286	−177.843	33.5	5.1	4.2	0.80	10	8	15.04	2.00	0.10	0.50	0.79	0.43
KS-D26															
1997/08/31	10:59:57.50	−30.287	−177.993	55.0	5.1	—	1.00	—	—	—	—	—	—	—	—
2004/02/01	23:12:45.60	−30.289	−177.992	55.0	5.1	6.4	0.80	18	10	9.52	−1.00	0.24	0.00	1.73	1.02
KS-D27															
2004/04/25	17:26:13.15	−30.289	−177.711	10.0	5.1	—	1.00	—	—	—	—	—	—	—	—
2004/11/17	10:43:55.26	−30.277	−177.706	9.7	5.3	0.6	0.81	24	17	31.05	20.00	1.42	−0.30	0.68	0.58
KS-D28															
2004/09/11	23:43:30.85	−30.642	−177.791	10.0	5.2	—	1.00	—	—	—	—	—	—	—	—
2009/10/31	20:34:48.86	−30.642	−177.792	10.0	4.9	5.1	0.80	11	6	36.02	38.60	0.10	0.00	0.53	0.20

(*continued*)

Table 2 (*Continued*)

Origin Date (yyyy/mm/dd)	Origin Time (hh:mm:ss.ss)	Latitude (°N)	Longitude (°E)	Depth (km)	m_b	dt (yr)	cc	N_{ph}	rms (ms)	dh_c (km)	dz_c (km)	dh_r (km)	dz_r (km)	$ellp_{maj}$ (km)	$ellp_{min}$ (km)
KS-D29															
2000/08/04	23:34:18.10	−31.454	−178.550	33.0	5.3	—	1.00	—	—	—	—	—	—	—	—
2009/04/03	14:37:55.87	−31.456	−178.550	33.2	5.3	8.7	0.82	24	14	5.82	21.60	0.22	0.20	0.91	0.44
VS-D1															
2008/07/09	02:34:43.00	−12.406	166.460	45.2	5.1	—	1.00	—	—	—	—	—	—	—	—
2009/10/15	19:20:14.47	−12.407	166.459	44.8	5.1	1.3	0.84	28	19	17.05	−10.20	0.16	−0.40	0.89	0.56
VS-D2															
2001/05/27	08:48:47.24	−19.589	168.851	33.0	5.5	—	1.00	—	—	—	—	—	—	—	—
2008/05/01	04:57:51.56	−19.590	168.851	33.0	5.7	6.9	0.90	44	8	13.42	2.00	0.11	0.00	1.11	0.78

The first event of each doublet refers to the reference (master) event with the origin time of the reference event fixed to that of the PDE catalog. The event-origin time of the second event is corrected for the origin-time error within the doublet as inferred from the master-event algorithm. m_b is body wave magnitude; dt is the time separation between the reference and second events in years (yr); cc is the average cross-correlation coefficient calculated by the number of seismic phases (N_{ph}) used for the master-event relocation; rms is the rms time residual within the doublet predicted based on the optimum location and depth of the second event relative to the reference event in milliseconds (ms); dh_c and dz_c are the horizontal and vertical separations within the doublet based on the PDE catalog; dh_r and dz_r are the horizontal and vertical separations within the doublet inferred from the master-event relocation; $ellp_{maj}$ and $ellp_{min}$ are the major and minor axes of the 95% confidence ellipse in the horizontal plane.

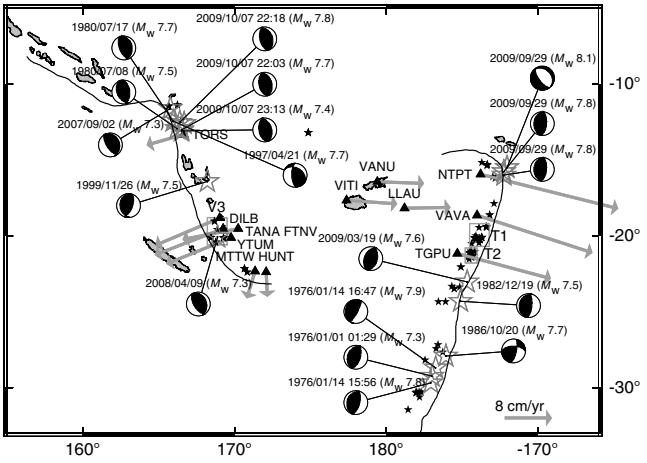

Figure 3. Large subduction-zone interplate earthquakes (large open gray stars) labeled with event date, M_w, GCMT focal mechanisms, and GPS velocity vectors (gray arrows and black triangles labeled with station name). GPS velocities are listed in Table 3. Black lines indicate the Tonga–Kermadec and Vanuatu trenches. Note that the 2009/09/29 Samoa–Tonga outer trench-slope event (M_w 8.1) triggered large interplate doublets (both of M_w 7.8; Lay *et al.*, 2010). The Pacific plate subducts westward beneath the Australian plate along the Tonga–Kermadec trench, whereas the Australian plate subducts eastward beneath the Vanuatu arc and North Fiji basin. The opposite orientation between the Tonga–Kermadec and Vanuatu subduction systems is due to complex and broad back-arc extension in the Lau and North Fiji basins (Pelletier *et al.*, 1998).

Fault-Slip Rate Inferred from the Scaling Relationship between Fault Slip (d) and Seismic Moment (M_0)

Nadeau and Johnson (1998) suggested that fault slip (d; cm) and M_0 (dyn·cm) for the repeaters in Parkfield on the SAF follow a log–log scaling relationship:

$$\log(d) = 0.17 \times \log(M_0) - 2.36. \qquad (2)$$

Table 3
GPS Velocities near the Tonga and Vanuatu Subduction Zones

Station	Latitude (°N)	Longitude (°E)	GPS Velocity Azimuth (N°E)	GPS Velocity (cm/yr)
NTPT	−15.947	−173.763	104	24
VAVA	−18.648	−173.999	108	20.5
TGPU	−21.173	−175.309	105	16.4
VANU	−16.432	179.413	92	7.9
VITI	−17.651	177.394	94	8.6
LLAU	−18.187	−178.78	89	7.8
TORS	−13.33	166.64	254	6.5
DILB	−18.82	169.02	247	11.8
TANA	−19.53	169.25	249	12.4
FTNV	−19.52	170.23	259	9.6
YTUM	−20.14	169.77	248	11.8
MTTW	−22.34	171.36	197	4.8
HUNT	−22.4	172.09	177	4.2

The listed GPS stations are near shallow repeaters in the Tonga and Vanuatu subduction zones. Note that GPS velocities are relative to the Australian Plate. GPS velocities were obtained from previous studies (Bevis *et al.*, 1995; Calmant *et al.*, 2003).

The main assumption in the derivation of equation (2) is that the tectonic loading rate is equal to the average fault-slip rate ($\dot{d}$). Igarashi *et al.* (2003), Uchida *et al.* (2003), and Chen *et al.* (2008) demonstrated that $\dot{d}$ estimated from equation (2) is applicable to the Chihshang fault in Taiwan and northeastern Japan, as calculated $\dot{d}$ values and its spatial distribution are consistent with the GPS data. As a first step towards understanding fault-slip rate in the Tonga–Kermadec–Vanuatu interplate regions, I use equation (2) to estimate fault slip and slip rate. A step increase in slip corresponds to the occurrence of an earthquake estimated from equation (2), and $\dot{d}$ is the slope between step increases in slip and time separation between two events (Fig. 9). Fault slip and slip rate may exhibit temporal variations due to aseismic slip associated with large interplate earthquakes or spatial variations such as transitions from strongly coupled to decoupled regions.

I primarily focus on the T1 and T2 plate-interface regions in Tonga and the V3 plate-interface region in Vanuatu, where there are several repeating earthquake clusters (Fig. 2). In the T1 region, the TS-C3, TS-C4, and TS-C7 clusters have a fairly constant $\dot{d}$ of 7.8, 20.5, and 8.1 cm/yr, respectively (Fig. 9a, Table 4). Moreover, the TS-C5 and TS-C6 clusters appear to have a temporal acceleration in $\dot{d}$. The TS-C5 cluster has $\dot{d}$ of 12 cm/yr before the 2003/10/09 event, followed by a $\dot{d}$ of 28 cm/yr for later events in the cluster. The TS-C6 cluster has $\dot{d}$ of 7.3 cm/yr before the 2002/02/15 event and a $\dot{d}$ of 19 cm/yr for later events in the cluster (Fig. 9a). In the T2 region, the TS-C8, TS-C9, TS-C10, and TS-C11 clusters have a consistent $\dot{d}$ in the range of 10–14 cm/yr (Fig. 9b, Table 4). In the V3 region, apart from the VS-C5 cluster, $\dot{d}$ accelerates after 2007 and 2008 for the VS-C3, VS-C4, and VS-C6 clusters (Fig. 9c). Among these clusters, the 2008/04/06 and 2008/06/01 events of the VS-C4 cluster and the 2008/04/10 event of the VS-C6 cluster are likely associated with the 2008/04/09 event (M_w 7.3; Figs. 2b, 3, and 9c). Near 165.7° E, 11.4° S in the northern Vanuatu plate-interface region, the burst-type VS-C2 and VS-D1 repeaters appear to have a temporal acceleration in $\dot{d}$ in the range 31–37 cm/yr (Fig. 2b, Table 4), which are probably associated with the aseismic afterslip of the 2007/09/02 M_w 7.3 event and the 2009/10/07 earthquake triplet (M_w 7.7, M_w 7.8, and M_w 7.4; Fig. 3). Average fault-slip rates $\dot{d}$ for each cluster and doublet are given in Table 4.

Estimation of Interplate Coupling

Interplate coupling is useful for identifying locked zones that could potentially produce large interplate earthquakes. The coupling coefficient (c) can be estimated based on the equation:

$$c = (V_0 - \dot{d})/V_0, \qquad (3)$$

for which V_0 is the GPS-derived plate convergence rate. A c of 0 indicates that the plate is creeping at its long-term slip rate, whereas a c of 1 indicates that the plate boundary is fully locked (Uchida, Nakajima, *et al.*, 2009). Previous studies

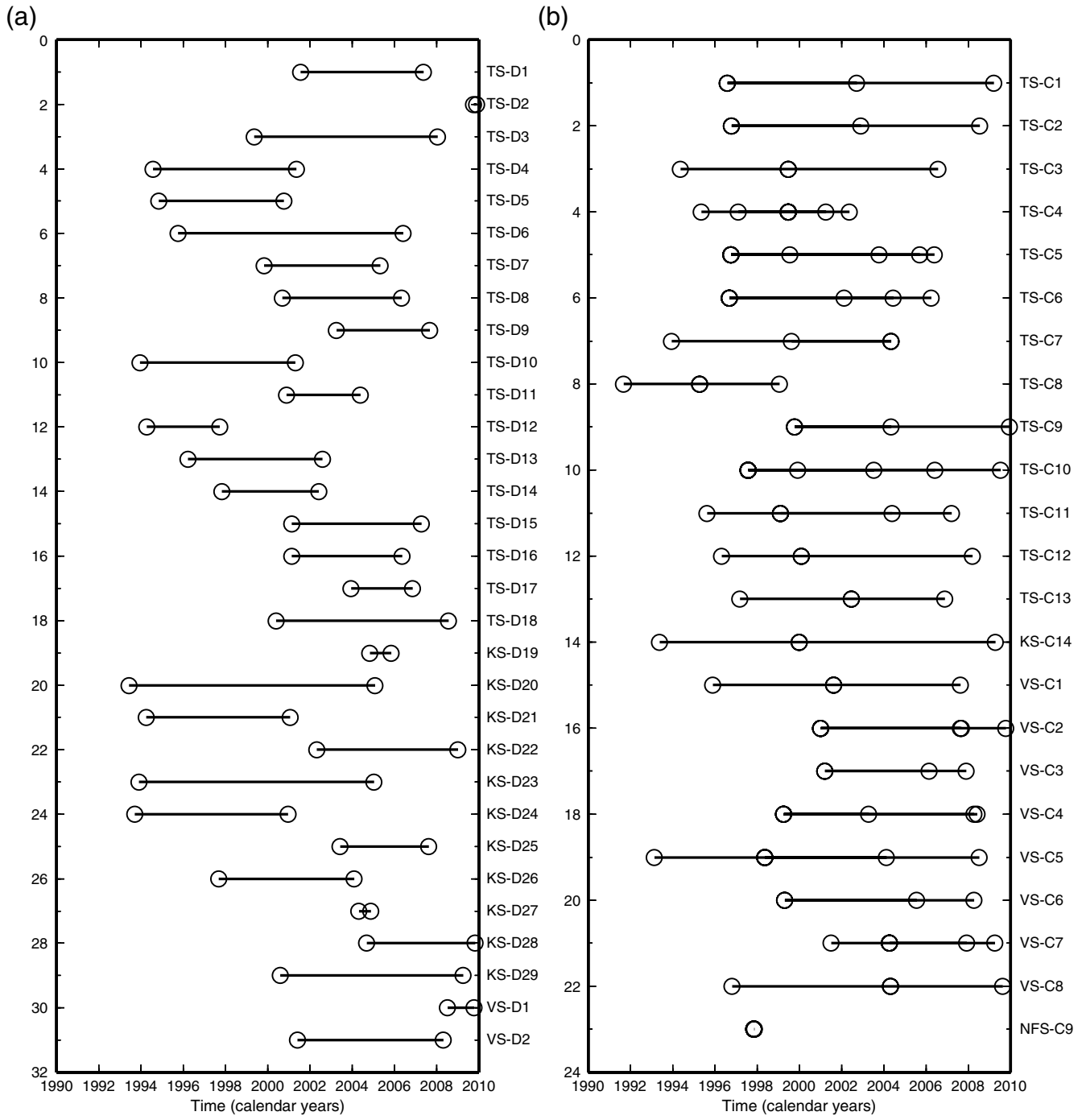

Figure 4. Time window for shallow-focus correlated earthquake (a) doublets and (b) clusters. The abbreviations S-D and S-C refer to Shallow Doublets and Shallow Clusters, respectively, whereas T, K, V, and NF refer to the regions Tonga, Kermadec, Vanuatu, and North Fiji basin, respectively.

analyzed GPS data and estimated convergence rate between the Pacific and Australian Plates along the Tonga and Vanuatu subduction zones (Bevis *et al.*, 1995; Calmant *et al.*, 2003; Table 3). A convergence rate of 8 cm/yr along the Kermadec subduction zone was adopted from the NUVEL-1 model (DeMets *et al.*, 1990). There were three GPS stations (NTPT, VAVA, and TGPU) along the 1500-km-long Tonga arc (Fig. 3, Table 3). Given that V_0 increases northward from 16.4 cm/yr at the TGPU station to 24.0 cm/yr at the NTPT station, I assigned V_0 for the clusters/doublets on the basis of the nearest GPS station. For example, several doublets and clusters in the T1 region are assigned with a V_0 of 20.5 cm/yr close to the VAVA station, and other clusters in the T1 region have a V_0 of 18.5 cm/yr as these are located between the VAVA and TGPU stations (Fig. 3, Tables 3 and 4). I noted that V_0 values quoted in the studies of Bevis *et al.*

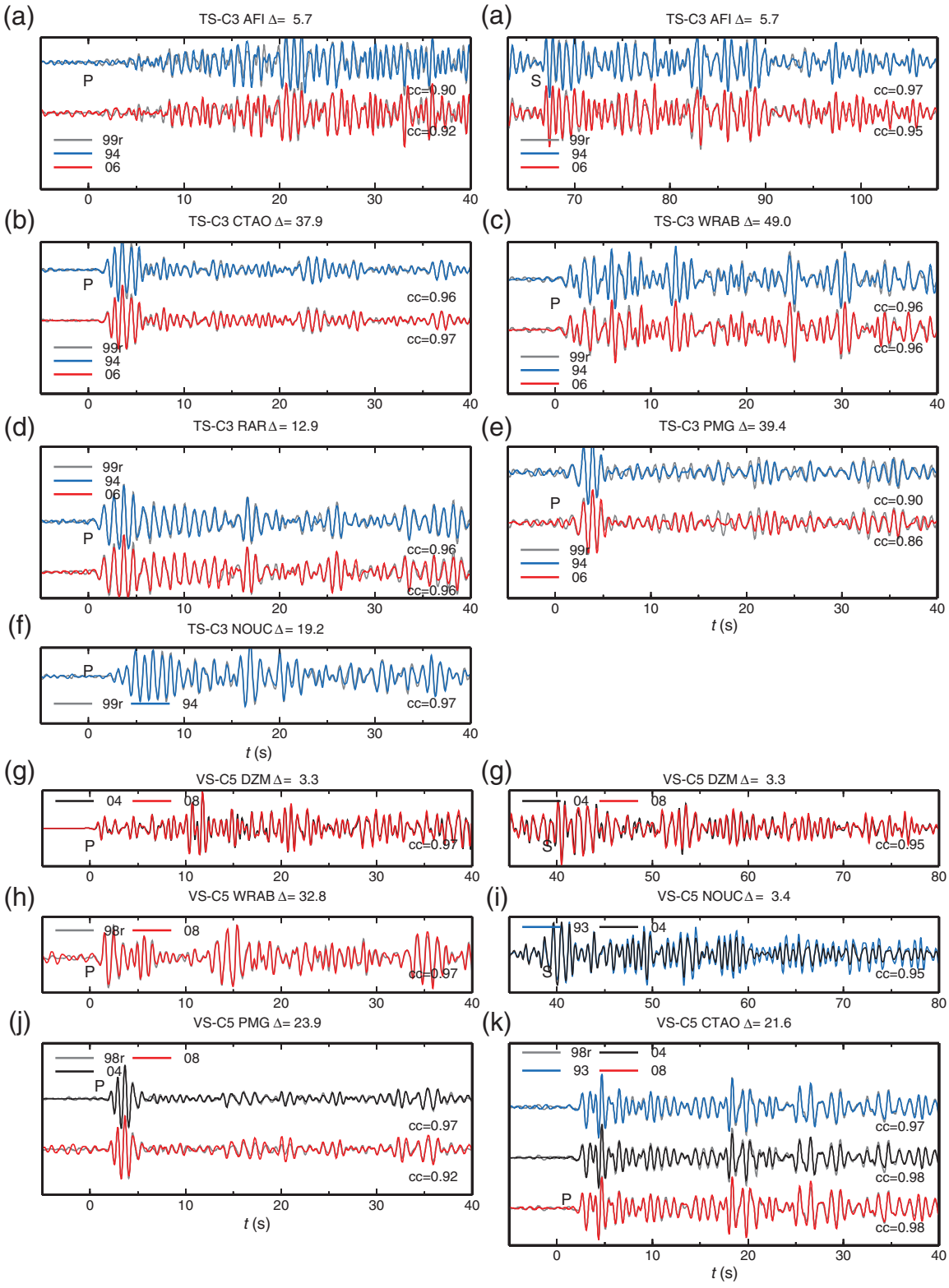

Figure 5. Examples of high-frequency waveforms filtered in the frequency range of 0.8–2.0 Hz for the TS-C3 cluster in Tonga recorded by the seismographs (a) AFI, (b) CTAO, (c) WRAB, (d) RAR, (e) PMG, and (f) NOUC and for the VS-C5 cluster in Vanuatu recorded by the seismographs (g) DZM, (h) WRAB, (i) NOUC, (j) PMG, and (k) CTAO. Epicentral distance (Δ) for each station is labeled at the top of each panel. Traces of the events are distinguished by different colors. (a, g) display both *P* and *S* coda, whereas the rest of the panels display only *P* coda, except (i), which only shows *S* coda. Note that cross-correlation (cc) coefficients of many traces with good SNRs can approach 0.85 and above, and the entire *P* and *S* coda are very similar (a, g).

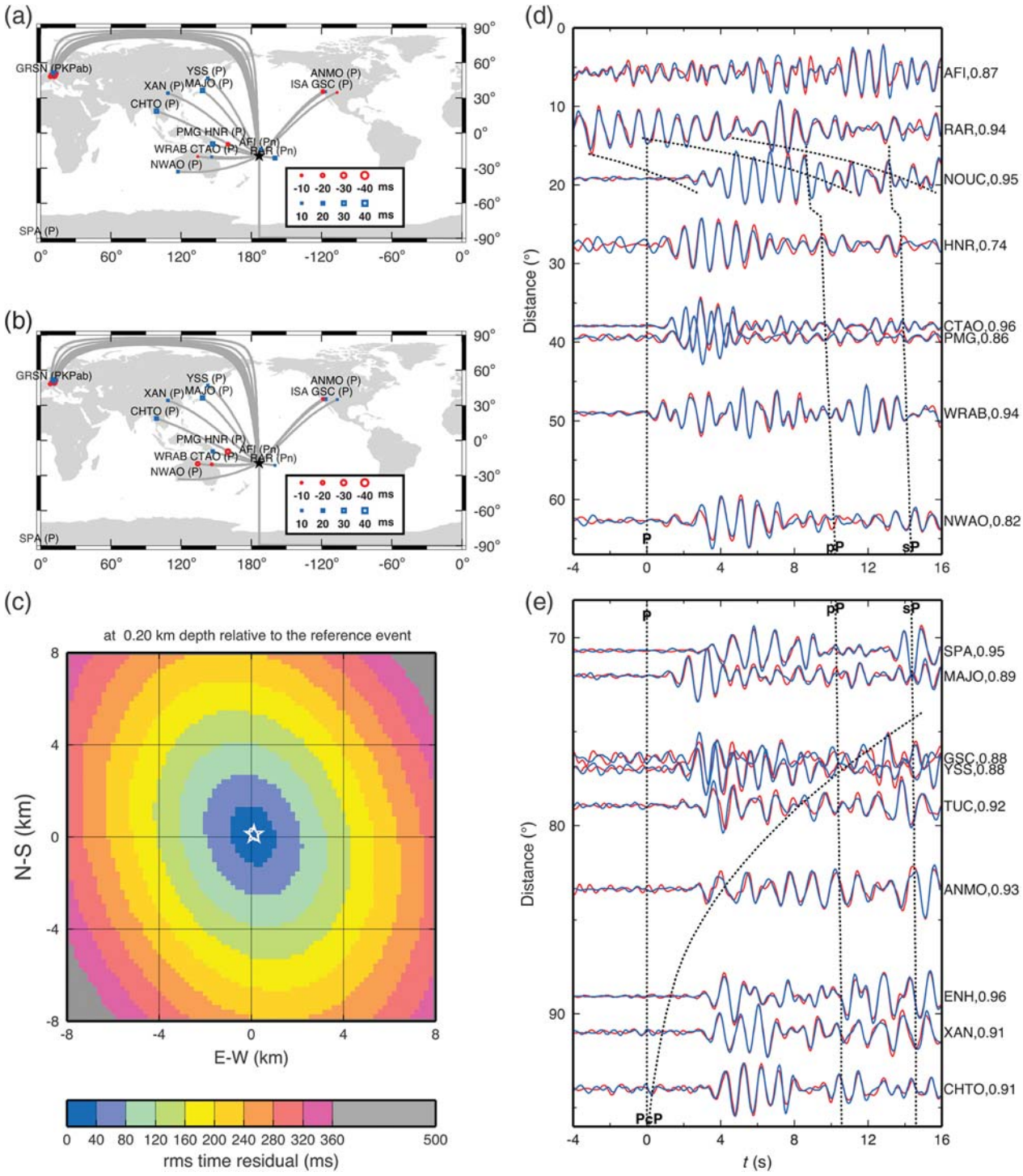

Figure 6. Relocation results and example waveforms for the 1999/06/21 (reference event, labeled as 99r) and 1994/05/15 (labeled as 94) events of the Tonga shallow cluster TS-C3, referred as TS-C3-99r-94 in the text. Regional *Pn* and teleseismic *P* and *PKP* phase pairs are used to determine the precise relative location. (a) Travel-time residuals subtracted from the mean of all travel-time residuals (the event origin time error) between the event pair plotted at the location of each seismograph, with the great circle paths (gray traces). (b) Predicted travel-time residuals based on the optimum location and depth of the second event relative to the reference (master) event plotted at the location of each seismograph. Negative and positive travel-time residuals are indicated by red circles and blue squares, respectively, and the magnitude of the travel-time residual is proportional to the size of the symbol. (c) rms time residual near the earthquake source. Coordinate (0, 0) corresponds to the location of the reference event. White open star corresponds to the optimum location and depth of the second event. White open ellipse corresponds to the 95% confidence ellipse calculated with 200 bootstrap re-samplings. (d, e) Examples of high-frequency *P*, *pP*, and *sP* waveforms filtered in the frequency range of 0.8–2.0 Hz for the 1999/06/21 (red traces) and 1994/05/15 (blue traces) earthquakes with station name and cc coefficient displayed on the right side of the panel. Waveforms for the reference event are aligned by the predicted *P* arrival of the IASP91 seismic velocity model (Kennett and Engdahl, 1991), whereas waveforms for the second event are aligned by waveform cc between the two traces.

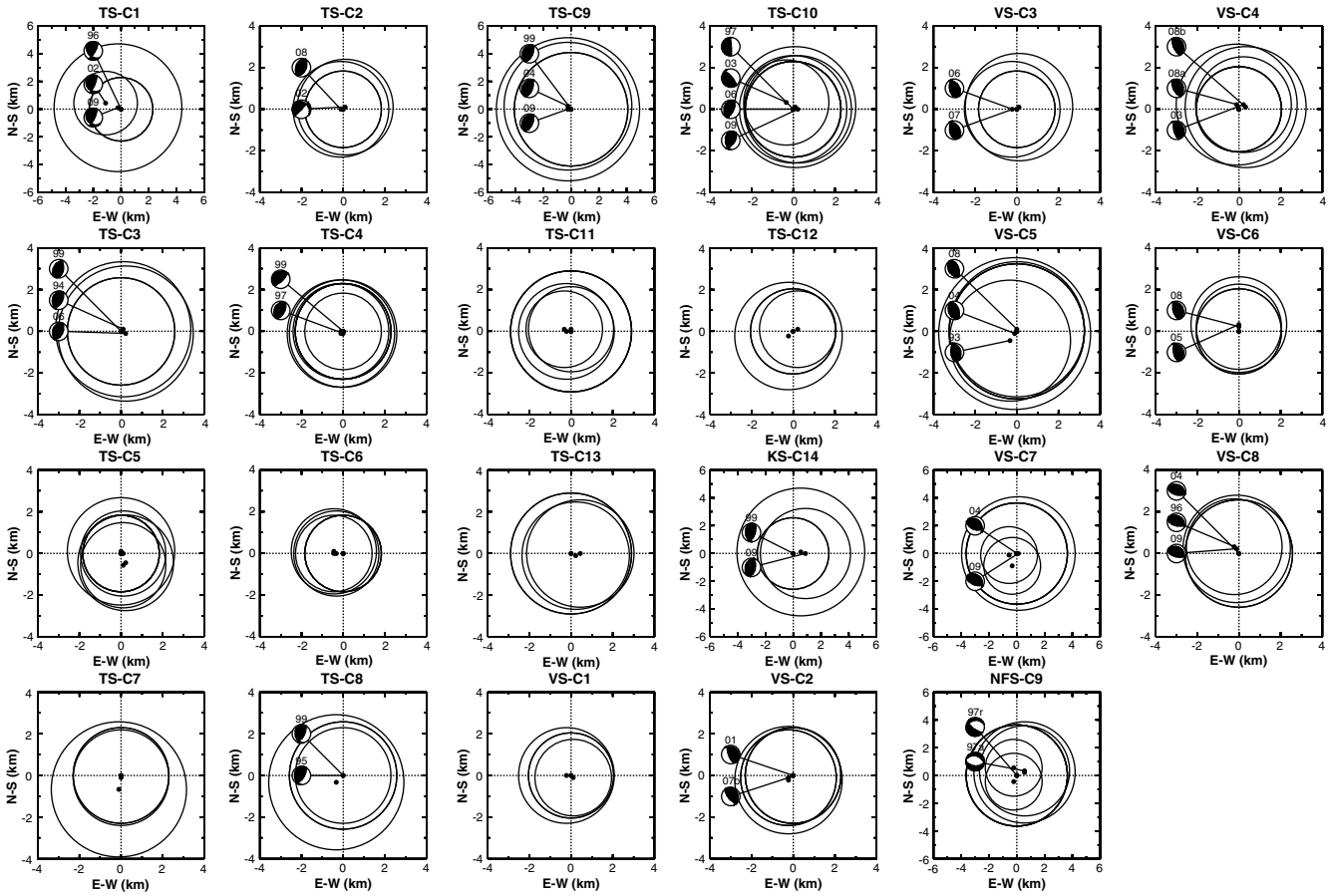

Figure 7. Relative locations for the 23 shallow-focus clusters in the Tonga–Kermadec–Vanuatu subduction zones. Each panel displays the east–west and north–south plane view for the clusters. Reference events of the clusters are located at coordinate (0, 0). Black circles refer to the estimated circular source areas. Only available GCMTs are plotted, which are labeled by year. Note that the difference in depth among the clusters is small (dz_r column in Table 1), thus only the east–west and north–south plane view is displayed. For some clusters, one or a few events slightly deviate from the rest of the events due to limited sampling coverage affecting determination of their precise relative location. In the VS-C2 cluster, 07b refers to the 2007/09/05 event. In the VS-C4 cluster, 08a and 08b refer to the 2008/04/06 and 2008/06/01 events, respectively. In the NFS-C9 cluster, 97r and 97a refer to the 1997/11/11 and 1997/11/03 events, respectively. Source parameters for the shallow-focus clusters are listed in Table 1.

(1995) and Calmant *et al.* (2003) were measured in the 1990s and early 2000s. It is possible that a temporal acceleration in slip rate may have occurred in the late 2000s. The effect of this would be to produce a smaller V_0 than $\dot{d}$ and a negative coupling coefficient.

Coupling coefficients exhibit regional variations in the Tonga, Kermadec, and Vanuatu plate-interface regions. In the northern part of Tonga (15°–19° S) plate-interface region, a high V_0 and a low $\dot{d}$ yield high coupling coefficients of 0.6–0.77 (Fig. 10a, Table 4). In the T1 and T2 regions, the coupling coefficients are usually <0.5 (Fig. 10b, Table 4). Along the Kermadec and Vanuatu plate-interface regions, the coupling coefficients are mostly <0.3, indicative of weak coupling or decoupling (Fig. 10a,c Table 4). Along the Vanuatu plate-interface region, many repeaters exhibit negative coupling coefficients due to an acceleration of aseismic slip caused by large interplate earthquakes (Fig. 10c, Table 4).

It should be noted that some plate-interface regions characterized by low background seismicity and a lack of repeating events are indicative of strong coupling that could not be resolved by this approach. For example, the following plate-interface regions are known to be strongly coupled inferred from the studies of large earthquakes and geodesy: near the junction of the Tonga–Kermadec subduction zones and the aseismic Louisville ridge (gray dashed regions labeled by LR in Fig. 10a; Christensen and Lay, 1988), and near Santo and Malekula where the aseismic D'Entrecasteaux ridge is subducting in the central Vanuatu region (gray dashed regions labeled by DER in Fig. 10c; Calmant *et al.*, 2003).

Scaling Relationship between Recurrence Interval (T_r) and Seismic Moment (M_0)

I now consider the recurrence time interval (T_r) among these clusters and doublets. T_r is defined as the average time difference between two successive events in a cluster. Following the notation used in the previous studies (Nadeau and Johnson, 1998; Chen *et al.*, 2008), a coefficient of

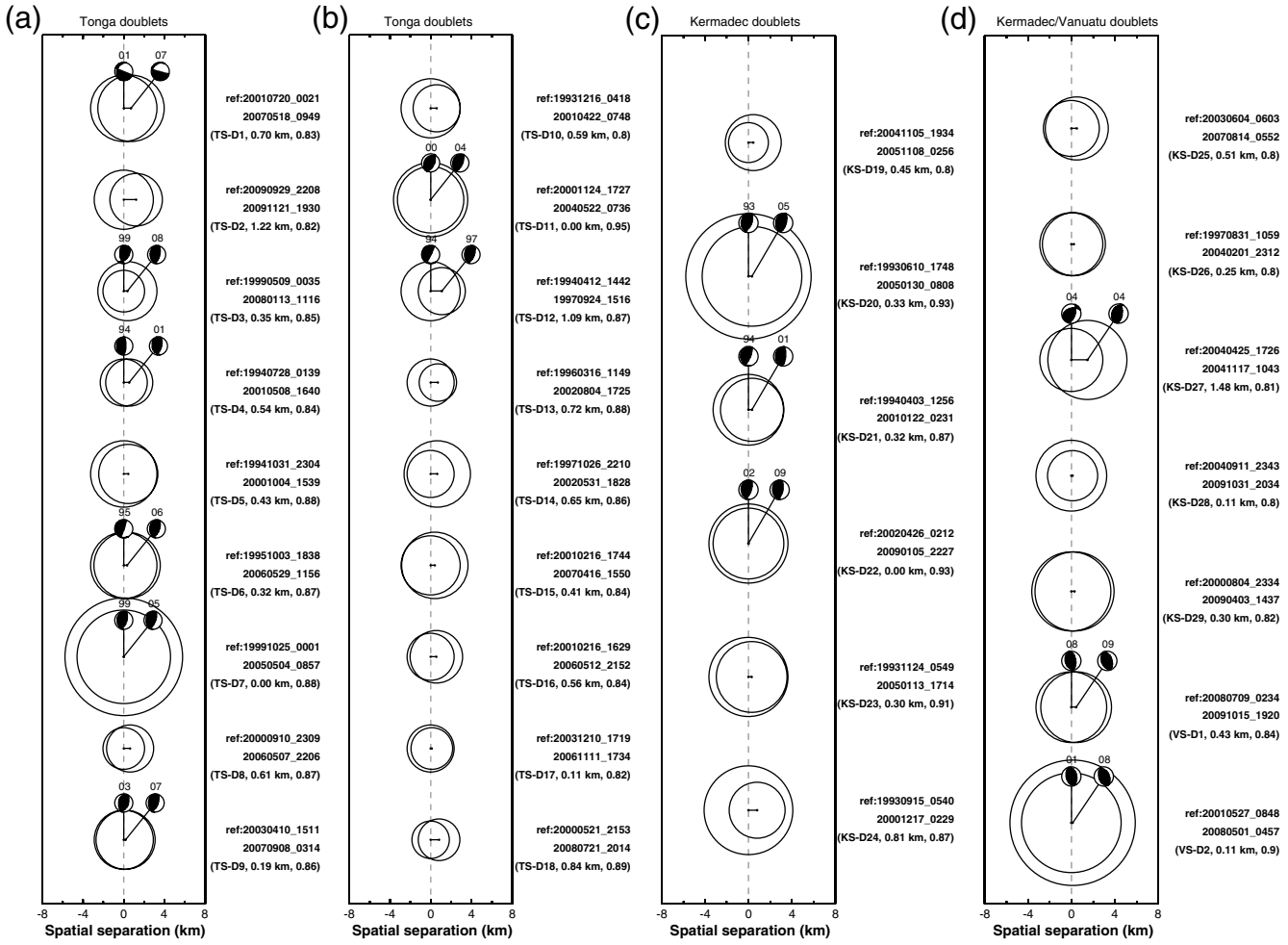

Figure 8. Spatial separation of the 31 shallow doublets in the Tonga–Kermadec–Vanuatu subduction zones. The reference events are placed at 0 km. Black circles refer to the estimated circular source areas of each earthquake. The size of the circular source areas is scaled on the basis of length of the x coordinate. On the right side of the panel, each doublet is labeled with the reference event id (ref, top row) and the second event id (middle row), and the doublet id, spatial separation in kilometers, and average cc coefficient (bottom row). Source parameters for the shallow doublets are displayed in Table 2. Note that the majority of the shallow clusters and doublets are defined as repeating earthquakes in that these similar earthquake pairs have comparable scalar moments and overlapping rupture areas.

variation (COV) is defined as the standard deviation divided by the mean. A COV for a recurrence interval of zero means the recurrence is perfectly periodic, whereas a COV in T_r of ~1.0 and a COV in $T_r > 1$ indicate Poisson recurrence and temporal clustering, respectively. COVs in T_r for the clusters are displayed in Figure 11. The majority of the clusters are quasi-periodic with a COV in $T_r < 0.5$. The acceleration of aseismic slip can promote the occurrence of events and produce a larger COV in T_r, such as the TS-C5, TS-C6, VS-C2, VS-C3, and VS-C4 clusters (Figs. 9 and 11). It is also reasonable to assume that the majority of the doublets are quasi-periodic.

Chen *et al.* (2007) studied the $T_r - M_0$ scaling relationship using data collected from small repeaters on the SAF, the Chihshang fault in Taiwan, and northeastern Japan. Chen *et al.* (2007) suggested that T_r and M_0 in the SAF also follow the log–log scaling relationship:

$$\log(T_r) = 0.16 \times \log(M_0) - 2.53, \quad (4)$$

for which T_r is in units of years and M_0 is in units of dyn·cm. Chen *et al.* (2007) observed that T_r measurements in northeastern Japan are four times shorter as compared with those on the SAF, and that T_r on the Chihshang fault are two times shorter as compared with T_r on the SAF. The differences in T_r between the SAF, the Chihshang fault, and northeastern Japan are due to variations in the geodetically derived long-term fault-slip rate (V_f). Chen *et al.* (2007) further suggested that the $T_r - M_0$ scaling relationship (equation 4) for Parkfield on the SAF can account for the normalized recurrence interval T_r (nor) for repeaters on the Chihshang fault and northeastern Japan, when T_r is normalized to Parkfield on the SAF by multiplying the normalization factor $V_f/V_{\text{Parkfield}}$:

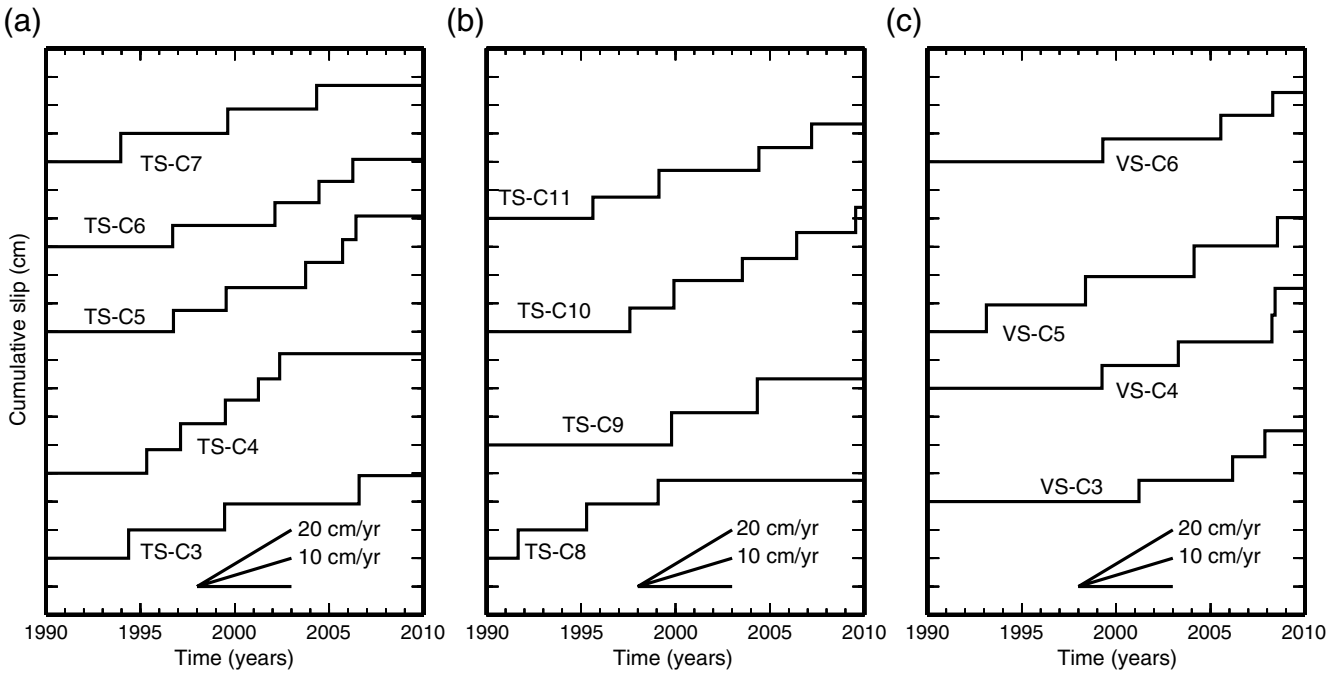

Figure 9. Cumulative slip (in cm) as a function of calendar time for the clusters in the (a) T1, (b) T2, and (c) V3 plate-interface regions in Tonga and Vanuatu (Fig. 2). A step increase in slip corresponds to the occurrence of an earthquake. Fault slip is estimated using equation (2). Fault-slip rate is the slope between slip increase and time separation between two events. Note that the TS-C5, TS-C6, VS-C3, VS-C4, and VS-C6 clusters appear to have a temporal acceleration in slip rate in the later part of the cluster.

$$T_r(\text{nor}) = T_r \times (V_f / V_{\text{Parkfield}}), \quad (5)$$

for which $V_{\text{Parkfield}}$ is the long-term fault-slip rate in Parkfield on the SAF with a value of 2.3 cm/yr. Chen *et al.* (2007) inferred that the tectonic loading rate is likely the most important factor that influences the repeat time of the earthquake cycle.

Moderate repeating earthquakes in the Tonga, Kermadec, and Vanuatu subduction zones can fill the data gap for larger M_0 and longer T_r, and provide measurements for different plate boundaries. Log (T_r) measurements for the moderate repeaters in the Tonga–Kermadec–Vanuatu subduction zones (black symbols) are below the predicted values from the scaling relationship (equation 4; dotted line) by 0.3 to 0.8 (Fig. 12a,b). This means that the time it takes for an earthquake to recur with the same M_0 is shorter in the Tonga–Kermadec–Vanuatu subduction zones than in Parkfield on the SAF by 2–6.3 yr. This result is expected because the convergence rates in Tonga (16–24 cm/yr; Bevis *et al.*, 1995), Kermadec (8 cm/yr; DeMets *et al.*, 1990), and Vanuatu (4–12 cm/yr; Calmant *et al.*, 2003; Table 3) are higher compared with the tectonic loading rate on the SAF (2.3 cm/yr). I compute the normalized recurrence interval T_r(nor) using equation (5). I assume that the average long-term fault-slip rate (V_f) is equal to the GPS-derived plate convergence rate (V_0; Table 4). This assumption may not be necessarily true, because GPS data only cover a short time period and likely represent a transient rate, and because the long-term interseismic slip rate could be unsteady. However, it is generally difficult to acquire long-term fault-slip rates from geodetic data in subduction zones. Given that the studies of Bevis *et al.* (1995) and Calmant *et al.* (2003) provide the only geodetic measurements in these areas, I begin with the assumption that $V_f = V_0$. The logarithm of the normalized recurrence interval log (T_r [nor]) for the interplate repeating earthquakes in the Kermadec and Vanuatu regions do, indeed, better fit the predicted value based on the scaling relationship (equation 4) as compared with log (T_r) (Fig. 12b,d). For the repeating earthquakes in the Tonga region, equation (4) does account for some, but not all, of the log (T_r [nor]) data (Fig. 12d). Note that equation (4) also assumes $V_0 = \dot{d}$, which presumes that the regions where the repeaters occurred are decoupled. This offers an explanation as to why equation (4) better matches log (T_r [nor]) in the Kermadec and Vanuatu interplate regions as compared with the Tonga interplate region (Fig. 12d). In order to understand the scatter in the log (T_r [nor]) data from the Tonga subduction zone, I isolate the log (T_r [nor]) data with high coupling coefficients of $\geq$0.7 (dark gray circles) from those with low coupling coefficients of $\leq$0.3 (light gray circles). Equation (4) can adequately explain the log (T_r [nor]) data with low coupling coefficients in Tonga (light gray circles in Fig. 12d), and the largest log (T_r [nor]) data values correspond to those with high coupling coefficients (dark gray circles in Fig. 12d). The $T_r - M_0$ measurements from the repeaters located at the weakly coupled or decoupled interplate regions in Tonga, Kermadec, and Vanuatu further confirm the scaling relationship (equation 4) derived from Parkfield on the SAF. My analyses provide further support

Table 4
Average Fault-Slip Rates ($\dot{d}$) Estimated from the Repeaters Compared with GPS-Derived Plate Convergence Rates (V_0) and Interplate Coupling Coefficients along the Tonga–Kermadec–Vanuatu Subduction Zones

Cluster Id/Doublet Id	$\dot{d}$ (cm/yr)	V_0 (cm/yr)	Interplate Coupling Coefficient
TS-C2	7.2	20.5	0.65
TS-C3	7.8	20.5	0.62
TS-C4	20.5	20.5	0
TS-C5	13.3	18.5	0.28
TS-C6	11.7	18.5	0.37
TS-C7	8.1	18.5	0.56
TS-C8	11.8	16.4	0.28
TS-C9	12.1	16.4	0.26
TS-C10	14.4	16.4	0.12
TS-C11	10.6	16.4	0.35
TS-C12	6.9	14	0.51
TS-C13	9.5	10	0.05
TS-D1	8.6	24	0.64
TS-D3	5.5	24	0.77
TS-D4	6.2	24	0.74
TS-D5	8	21	0.62
TS-D6	4.7	20.5	0.77
TS-D7	12.2	20.5	0.4
TS-D8	7.5	18.5	0.59
TS-D9	10.8	18.5	0.42
TS-D10	5.7	18.5	0.69
TS-D11	14.4	18.5	0.22
TS-D15	8.2	16.4	0.5
TS-D16	8.6	16.4	0.48
TS-D17	13.6	10	−0.36
TS-D18	4.9	10	0.51
KS-D20	5.2	8	0.35
KS-D21	7	8	0.12
KS-D22	7.2	8	0.1
KS-D23	4.5	8	0.44
KS-D25	11.3	8	−0.41
KS-D26	7.4	8	0.07
KS-D29	6.2	8	0.22
VS-C1	7	6.5	−0.08
VS-C2	14.3	6.5	−1.2
VS-C3	12	11.8	−0.02
VS-C4	10	11.8	0.15
VS-C5	9.9	11.8	0.16
VS-C6	8.7	11.8	0.26
VS-C8	6.9	4.8	−0.44
VS-D1	37.4	6.5	−4.75
VS-D2	9.8	11.8	0.17

Note that the average fault-slip rate ($\dot{d}$) is derived from least squares fitting the slip for each event throughout the cluster or doublet. For several clusters and doublets, a negative coupling coefficient is likely a result of temporal acceleration of aseismic slip.

for the conclusions of Chen *et al.* (2007) that the plate convergence rate is the predominant influence on the recurrence interval in a sequence.

A Cluster in the North Fiji Basin

The NFS-C9 cluster occurred in the North Fiji basin at a depth of about 11 km and was characterized by normal-fault focal mechanisms and a short time separation of days. In fact, the NFS-C9 cluster belongs to an earthquake swarm consisting of 14 earthquakes with m_b of 4.8–5.3, which occurred over a one month period in the North Fiji basin in November 1997. In the same area, there is another normal-fault earthquake swarm consisting of 15 events with m_b 4.8–5.8 in March 1993. Other event pairs within the 1993 or 1997 swarms and event pairs between the 1993 and 1997 swarms yield considerably lower cc coefficients, apart from the pair 1997/11/11 and 1997/11/06 with a cc coefficient of 0.76 (Table 1). Moreover, some events of the NFS-C9 cluster are not exactly overlapping (NFS-C9 in Fig. 7). The NFS-C9 cluster is probably associated with active ridge spreading, in that the epicenter and the direction of the *T*-axis of the NFS-C9 cluster geographically correspond to the location and the spreading direction of the North Spreading ridge of the North Fiji basin (Pelletier *et al.*, 1998). The episodic occurrence, short time separation, normal faulting, and shallow hypocentral depth for the NFS-C9 cluster mimic those for the ridge-spreading earthquake swarm in the northern Gulf of California (Thatcher and Brune, 1971).

Discussion

Comparison with Previous Studies

Zhang *et al.* (2008) searched for repeating earthquakes in the Tonga–Kermadec–Vanuatu subduction zones. The repeaters discovered in the paper of Zhang *et al.* (2008) are also found by waveform cross correlation in my paper. I note that there are several differences in the database and procedures used by Zhang *et al.* (2008) and my paper: (1) Zhang *et al.* (2008) used an m_b of 5.0, whereas I use an m_b of 4.7 as the lower bound of the magnitude threshold; (2) the waveform data of Zhang *et al.* (2008) were collected between January 1991 and January 2005, whereas I include waveforms for events up to December 2009, which encompasses almost five years more data collection than the paper of Zhang *et al.* (2008). A longer time window is advantageous in identifying more repeating earthquakes in the cluster and also allows the $T_r - M_0$ scaling relationship, fault-slip rate ($\dot{d}$), and coupling coefficient to be studied; (3) Zhang *et al.* (2008) detected similar earthquake pairs by cross-correlating waveforms recorded by a single seismic station CTAO, whereas I cross correlate waveform pairs recorded by all available stations of the GSN and several regional seismic networks. I determine the precise relative location among the similar earthquake pairs, estimate the size of the circular source rupture areas, and superpose the source rupture areas relative to the precise relative location to ensure that the correlated earthquake pairs are repeating earthquakes. Finally, I note that some correlated earthquake pairs that occurred between 1991 and 1992 which were identified in the paper of Zhang *et al.* (2008) are not considered in my paper, because those earthquake pairs have few travel-time measurements and their precise relative location is less well determined.

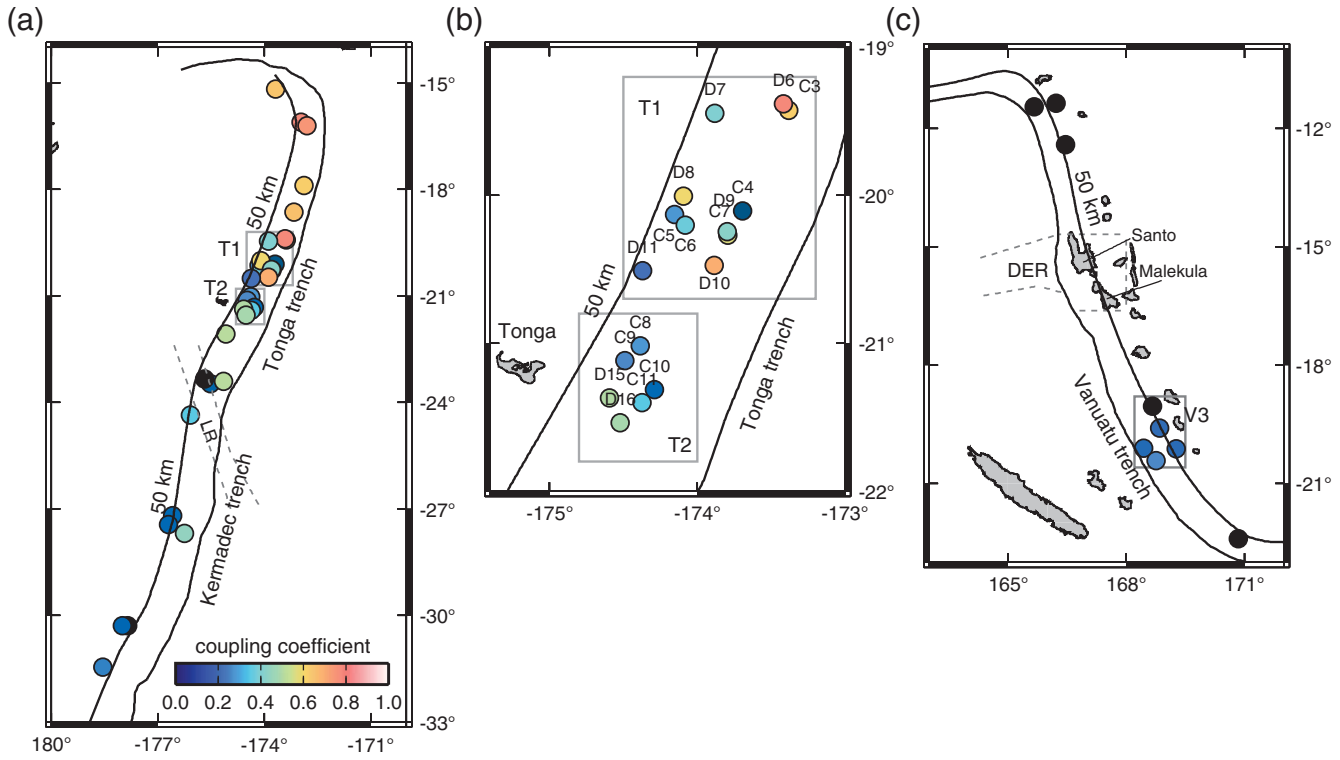

Figure 10. Spatial distribution of interplate coupling coefficients for each cluster and doublet. (a) Tonga–Kermadec interplate region, (b) expanded view of the T1 and T2 interplate regions in Tonga, and (c) Vanuatu interplate region. In (b), both cluster id and doublet id are labeled. Strong coupling (coupling coefficient $\geq$0.7) observed in the Tonga plate-interface region is apparently at odds with that expected in the presence of active back-arc opening in the Lau basin. Note that in (a, c), the strongly coupled plate-interface regions bounded by gray dashed lines are previously inferred from the studies of large earthquakes and geodesy. These strongly coupled plate-interface regions are characterized by the subduction of the aseismic Louisville ridge (LR; a) and the D'Entrecasteaux ridge (DER; c).

Uncertainties in the Estimation of Fault-Slip Rate

Uncertainties in $\dot{d}$ influence the values of the coupling coefficient and normalized recurrence interval T_r (nor). I now consider several likely sources of uncertainty that can affect the estimation of $\dot{d}$. One possible source of uncertainty is a temporal change in aseismic slip, such as observed in the TS-C5, TS-C6, and VS-C6 clusters. For example, the acceleration in aseismic slip for the TS-C5 cluster is 28 cm/yr following the 2003/10/09 event, but the average measured $\dot{d}$ is 13.3 cm/yr for the cluster (Table 4). The actual uncertainty depends on the magnitude of aseismic slip. Another possible uncertainty is missing event(s) in the clusters (Uchida and Matsuzawa, 2011) and measurements from the doublets. A missing event could alter $\dot{d}$, whereas a doublet yields a slip rate of about 2–3 cm/yr lower as compared with that estimated from the cluster in the same region (e.g., TS-C3 versus TS-D6, and TS-C11 versus TS-D15; Table 4, Fig. 10b). The other likely uncertainty emerges from the $d - M_0$ scaling relationship (equation 2), because the assumption used in the derivation of equation (2) is that the tectonic loading rate is equal to the slip rate. For strongly coupled regions (i.e., $V_0 > \dot{d}$), the $d - M_0$ scaling relationship may not conform to equation (2) and could also alter $\dot{d}$.

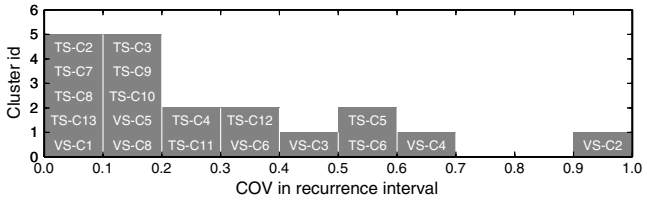

Figure 11. Coefficient of variation (COV) for the recurrence intervals (T_r) of 19 shallow clusters in the Tonga–Kermadec–Vanuatu plate-interface regions. The majority of the clusters are quasi-periodic with COV in $T_r < 0.5$. Note that the TS-C1, KS-C14, VS-C7, and NFS-C9 clusters are excluded, because the source areas are not comparable for events of the TS-C1, KS-C14, and VS-C7 clusters (Fig. 7), and because the NFS-C9 cluster exhibits temporal clustering (Fig. 4b).

Possible Explanations for Strong Interplate Coupling in the Northern Tonga

It is generally thought that subduction zones associated with active back-arc extension are weakly coupled or decoupled, such as the Mariana and Tonga subduction zones (Uyeda and Kanamori, 1979). Several subsequent studies have attempted to quantify seismic coupling along major subduction zones worldwide. Peterson and Seno (1984) estimated that seismic coupling coefficients were 0.08, 0.13, and 0.16 for the Tonga, Kermadec, and Vanuatu interplate regions, respectively, whereas Pacheco *et al.* (1993) obtained

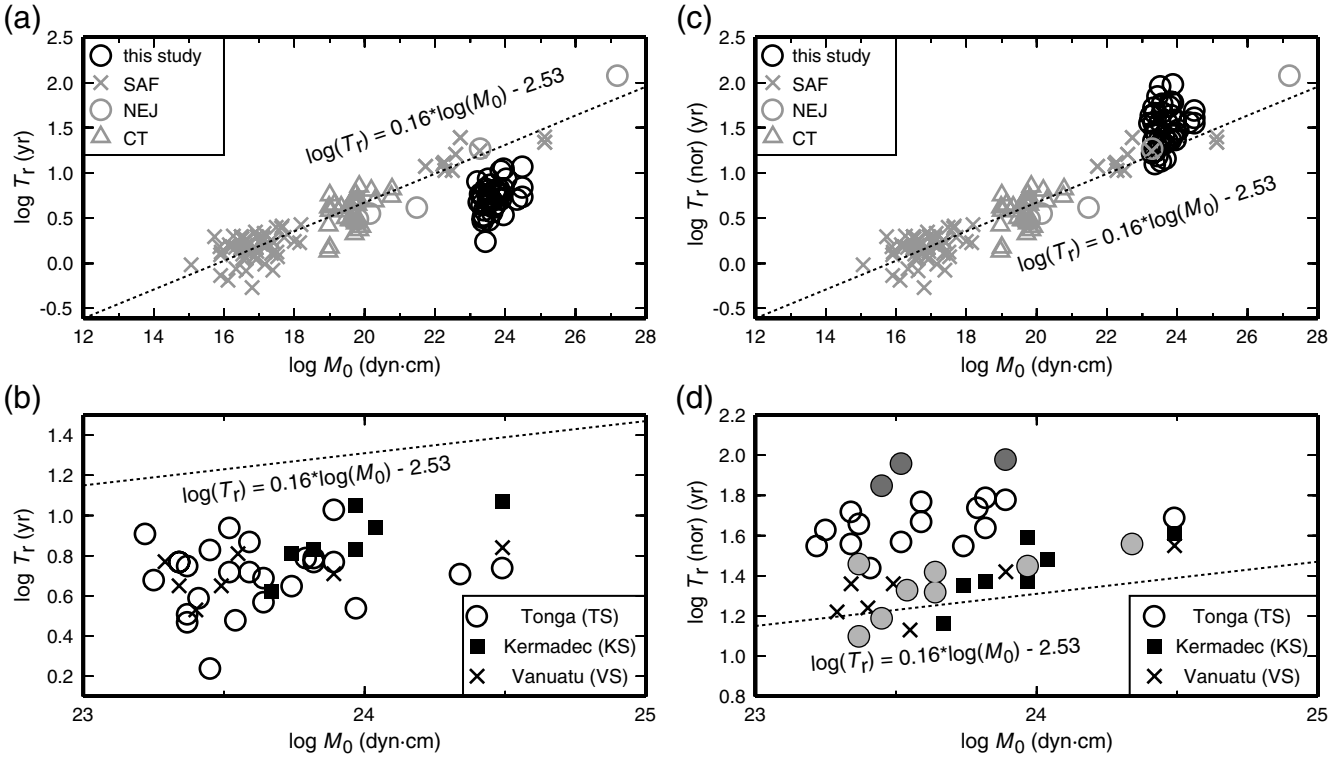

Figure 12. (a) $T_r - M_0$ measurements for shallow repeating earthquakes in the Tonga, Kermadec, and Vanuatu interplate regions (black open circles, labeled as this study) compared with those made for the San Andreas fault (SAF; gray crosses), northeastern Japan (NEJ; gray circles), the Chihshang fault in Taiwan (CT; gray triangles). Equation (4) ($\log(T_r) = 0.16 \times \log(M_0) - 2.53$) was derived from fitting the $T_r - M_0$ measurements from Parkfield on the SAF published in Chen *et al.* (2007). (b) Expanded view displaying the $T_r - M_0$ measurements for the Tonga (black open circles), Kermadec (black solid squares), and Vanuatu (black crosses) interplate regions. (c) and (d) are as analogous to (a) and (b), respectively, except T_r for the repeaters in the Tonga–Kermadec–Vanuatu regions is normalized to the average long-term fault-slip rate from Parkfield on the SAF by multiplying the normalization factor $V_f/V_{\text{Parkfield}}$ as in equation (5), which are labeled as T_r(nor). In (d), for the log (T_r [nor]) data from the Tonga region, dark gray and light gray circles correspond to the repeaters with high ($\geq$0.7) and low ($\leq$0.3) coupling coefficients, respectively. $T_r - M_0$ measurements for the repeaters in the interplate regions with low coupling coefficients are better explained by equation (4).

seismic coupling coefficients of 0.38, 0.16, and 0.13 for the Tonga, Kermadec, and Vanuatu interplate regions, respectively, from a seismicity record of 90 yr. Although these two studies adopted slightly different methods to estimate seismic coupling coefficients, they are in agreement that the majority of the Tonga, Kermadec, and Vanuatu interplate boundaries are weakly coupled, except for those interplate boundaries near the subduction of the aseismic ridge as stated previously.

The weak coupling of the Kermadec and Vanuatu interplate regions, and in the southern section 20°–23° S of the Tonga interplate region is generally consistent with the studies of Peterson and Seno (1984) and Pacheco *et al.* (1993; Fig. 10). However, high coupling coefficients (i.e., strongly coupled) in the northern section 15°–19° S of the Tonga interplate region are inconsistent with the previous studies. I provide several possible explanations for this discrepancy. First, this part of the interplate boundary is in fact strongly coupled. In particular, the great 2009 Samoa–Tonga outer trench-slope event (M_w 8.1) followed by large interplate doublets (both of M_w 7.8; Lay *et al.*, 2010) provides compelling evidence for the northern Tonga interplate region being strongly coupled. In addition, compared with the multitude of repeaters in the regions T1 and T2, the lack of repeaters in the northern Tonga interplate region may also be an indication of strong coupling. On the other hand, the aseismic slip could also be existent in other forms of slow earthquakes and small repeaters that cannot be quantified by this paper. The aseismic slip and slip rate estimated from moderate repeating earthquakes and equation (2) could be underestimated compared to the total aseismic slip, thereby producing a larger coupling coefficient.

Possible Explanations for Variations in the $T_r - M_0$ Scaling Relationship

The $T_r - M_0$ scaling relationship (equation 4) derived from the SAF is able to account for the T_r (nor)–M_0 data for the repeating earthquakes that have occurred in northeastern Japan, on the Chihshang fault, in the Kermadec and Vanuatu interplate regions, and in part of the Tonga interplate region. However, there are apparent variations in the T_r (nor) data for the Tonga region. In this section, I explore the factors that could contribute to the variations

in the T_r (nor) data. Assuming a circular rupture area, constant stress drop ($\Delta\sigma$), and no aseismic slip, the $T_r - M_0$ relationship for the repeating events should follow the relationship $T_r \propto M_0^{\frac{1}{3}}$ (Beeler *et al.*, 2001). Small repeating events observed in Parkfield on the SAF reveal a weaker $T_r - M_0$ dependency of $T_r \propto M_0^{\frac{1}{6}}$ (Nadeau and Johnson, 1998). To explain the discrepancy between the expected and observed $T_r - M_0$ data, researchers have developed several possible models including high stress drop ($\Delta\sigma$; Nadeau and Johnson, 1998; Sammis *et al.*, 1999), V_0 not being equal to $\dot{d}$, the repeaters occurring at the border between locked and adjacent creeping zones (Anooshehpoor and Brune, 2001; Sammis and Rice, 2001; Johnson and Nadeau, 2002), and the occurrence of aseismic slip (Beeler *et al.*, 2001). Some of these explanations may provide insight as to how to interpret the variations in the $T_r - M_0$ data. Assuming a constant tectonic loading rate, in order to yield $T_r \propto M_0^{\frac{1}{6}}$, it requires that $\Delta\sigma$ has a dependency on M_0 (i.e., $\Delta\sigma \propto M_0^{-\frac{1}{4}}$). Small repeating events thus could have very high stress drop (Nadeau and Johnson, 1998; Chen *et al.*, 2007). The variations in the log (T_r[nor]) data in the range of 23–24 of log (M_0) appear to be independent of M_0 (Fig. 12d). The high stress-drop model is thus unlikely to account for the variations in the $T_r - M_0$ data. I consider that V_0 not being equal to $\dot{d}$, and the occurrence of aseismic slip, are both likely to account for the variations in the $T_r - M_0$ data. Aseismic slip could lengthen or shorten T_r measured by moderate repeaters and produce varying T_r compared with the T_r calculated from equation (4). Moreover, the largest log (T_r[nor]) data values in the Tonga region correspond to those with strong coupling (i.e., $V_0 > \dot{d}$), which do not conform to the assumption $V_0 = \dot{d}$ in deriving the $T_r - M_0$ scaling relationship (equation 4). The fact that the repeaters occurred in a location where V_0 is not equal to $\dot{d}$ provides a plausible explanation for the variations of T_r (nor). Finally, I note that T_r(nor) is computed using the normalization factor $V_f/V_{\text{Parkfield}}$ using the assumption of $V_f = V_0$. The large log (T_r[nor]) data values could be due to an overestimation of V_f. Clearly, it remains challenging to robustly estimate the long-term fault-slip rate in subduction zones.

Conclusions

I have collected a large waveform dataset for moderate shallow-focus earthquakes that have occurred in the Tonga–Kermadec–Vanuatu subduction zones and were teleseismically recorded by the GSN and regional seismic networks between 1990 and 2009. I have identified a total of 23 clusters and 31 doublets with an average cc coefficient of >0.8 among $>390,000$ potential pairs. These highly correlated clusters and doublets have occurred at the plate interface and are characterized by low-angle thrust-type focal mechanisms. The majority of these highly correlated event pairs are repeating earthquakes, as defined by their similar seismic moments and completely overlapping source areas. Most repeating earthquakes are continual-type, with a recurrence interval on the order of years, and are quasi-periodic with COV in $T_r < 0.5$. I also observed burst-type repeaters, such as the VS-C2 and VS-C4 clusters, associated with large interplate earthquakes in the Vanuatu region. The burst-type nature is reflected by a large COV in T_r of >0.5 and a temporal acceleration in $\dot{d}$.

These repeating events are used to examine the $T_r - M_0$ scaling relationship, derived from Parkfield on the SAF, and to estimate spatial–temporal changes in $\dot{d}$ using the $d - M_0$ scaling relationship derived from the SAF, and the state of interplate coupling. The continual-type repeating clusters exhibit a reasonably constant $\dot{d}$, whereas the burst-type repeaters reveal a temporal acceleration in $\dot{d}$. My analyses reveal spatial–temporal variations in $\dot{d}$ in the Tonga–Kermadec–Vanuatu interplate regions. The results of my paper reveal weak coupling in the Kermadec, Vanuatu, and the southern section of the Tonga (20°–23° S) interplate regions, and strong coupling in the northern section of the Tonga (15°–19° S) interplate region. Strong coupling in the northern Tonga interplate region contrasts with the general understanding of the decoupled plate boundaries undergoing active back-arc extension in the Lau basin. The $T_r - M_0$ scaling relationship derived from the SAF can reasonably account for T_r(nor) for repeaters that have occurred in the Kermadec, Vanuatu, and the Tonga interplate boundaries where it is decoupled. This observation suggests that the convergence rate is the predominant influence on the repeat time in an earthquake sequence.

Data and Resources

My seismic data were collected from the Global Seismographic Network (GSN), the Global Telemetered Seismograph Network (GT), GEOSCOPE (G), the new China Digital Seismograph Network (CD, IC), the Caltech Regional Seismic Network (CI), the United States National Seismic Network (US) from the Incorporated Research Institutions for Seismology Consortium Data Management Center (http://www.iris.edu/hq/), the German Regional Seismic Network and the Gräfenberg Seismic Network from the SZGRF (http://www.szgrf.bgr.de/), and the Canadian National Seismographic Network (http://earthquakescanada.nrcan.gc.ca/stnsdata/wf_index-eng.php). Earthquake focal mechanisms were obtained from the Global Centroid Moment Tensor Project (www.globalcmt.org/CMTsearch.html). Figures were prepared using the Generic Mapping Tools software (Wessel and Smith, 1998) available at http://www.soest.hawaii.edu/gmt/. Seismic Analysis Code software was used to process the seismic data. The aforementioned web links were last accessed in February 2012.

Acknowledgments

I acknowledge helpful discussions with Masataka Ando, Kate Huih-suan Chen, Lee Chow, Ya-Ju Hsu, Bor-Shouh Huang, Shiann-Jong Lee,

Laetitia Mozziconacci, Teh-Ru Alex Song, Lianxing Wen, Wen-Nan Wu, and Li Zhao. Constructive comments and suggestions by the reviewers helped to clarify various points and improve this manuscript. The master-event algorithm software was provided by Lianxing Wen. $T_r - M_0$ data compilations for repeating earthquakes in the SAF, the Chihshang fault, and northeastern Japan were provided by Kate Huihsuan Chen. Some parts of the relocation calculations were carried out by Yi-Jung Lin. This paper was supported by the Institute of Earth Sciences, Academia Sinica, Taiwan, and the National Science Council, Taiwan under the Grants NSC-99-2116-M-001-003-, NSC-100-2119-M-001-018-, and NSC-101-2116-M-001-023-.

References

Anooshehpoor, A., and J. N. Brune (2001). Quasi-static slip-rate shielding by locked and creeping zones as an explanation for small repeating earthquakes at Parkfield, *Bull. Seismol. Soc. Am.* **91,** 401–403.

Beeler, N. M., D. L. Lockner, and S. H. Hickman (2001). A simple stick-slip and creep-slip model for repeating earthquakes and its implication for microearthquakes at Parkfield, *Bull. Seismol. Soc. Am.* **91,** 1797–1804.

Bevis, M., F. W. Taylor, B. E. Schutz, J. Recy, B. L. Isacks, S. Helu, R. Singh, E. Kendrick, J. Stowell, B. Taylor, and S. Calmant (1995). Geodetic observations of very rapid convergence and back-arc extension at the Tonga arc, *Nature* **374,** 249–251.

Bird, P. (2003). An updated digital model of plate boundaries, *Geochem. Geophys. Geosyst.* **4,** no. 1027, 52, doi: 10.1029/2001GC000252.

Brune, J. N. (1970). Tectonic stress and spectra of seismic shear waves from earthquakes, *J. Geophys. Res.* **75,** 4997–5009.

Calmant, S., B. Pelletier, P. Lebellegard, M. Bevis, F. W. Taylor, and D. A. Phillips (2003). New insights on the tectonics along the New Hebrides subduction zone based on GPS results, *J. Geophys. Res.* **108,** no. 2319, 22, doi: 10.1029/2001JB000644.

Chao, K., and Z. G. Peng (2009). Temporal changes of seismic velocity and anisotropy in the shallow crust induced by the 1999 October 22 *M* 6.4 Chia-Yi, Taiwan earthquake, *Geophys. J. Int.* **179,** no. 3, 1800–1816, doi: 10.1111/j.1365-246X.2009.04384.x.

Chen, K. H., T. Furumura, J. Rubinstein, and R. J. Rau (2011). Observations of changes in waveform character induced by the 1999 M_w 7.6 Chi-Chi earthquake, *Geophys. Res. Lett.* **38,** no. L23302, 5, doi: 10.1029/2011GL049841.

Chen, K. H., R. M. Nadeau, and R. J. Rau (2007). Towards a universal rule on the recurrence interval scaling of repeating earthquakes? *Geophys. Res. Lett.* **34,** no. L16308, 5, doi: 10.1029/2007GL030554.

Chen, K. H., R. M. Nadeau, and R. J. Rau (2008). Characteristic repeating earthquakes in an arc-continent collision boundary zone: The Chihshang fault of eastern Taiwan, *Earth Planet. Sci. Lett.* **276,** nos. 3–4, 262–272, doi: 10.1016/j.epsl.2008.09.021.

Chen, K. H., R. J. Rau, and J. C. Hu (2009). Variability of repeating earthquake behavior along the Longitudinal Valley fault zone of eastern Taiwan, *J. Geophys. Res.* **114,** no. B05306, 16, doi: 10.1029/2007JB005518.

Cheng, X., F. L. Niu, P. G. Silver, S. Horiuchi, K. Takai, Y. Iio, and H. Ito (2007). Similar microearthquakes observed in western Nagano, Japan, and implications for rupture mechanics, *J. Geophys. Res.* **112,** no. B04306, 13, doi: 10.1029/2006JB004416.

Christensen, D. H., and T. Lay (1988). Large earthquakes in the Tonga region associated with subduction of the Louisville Ridge, *J. Geophys. Res.* **93,** 13,367–13,389.

DeMets, C., R. G. Gordon, D. F. Argus, and S. Stein (1990). Current plate motions, *Geophys. J. Int.* **101,** 425–478.

Dziewoński, A. M., T. A. Chou, and J. H. Woodhouse (1981). Determination of earthquake source parameters from waveform data for studies of global and regional seismicity, *J. Geophys. Res.* **86,** 2825–2852.

Ekström, G., A. M. Dziewoński, N. N. Maternovskaya, and M. Nettles (2003). Global seismicity of 2001: Centroid-moment tensor solutions for 961 earthquakes, *Phys. Earth Planet. In.* **136,** nos. 3–4, 165–185, doi: 10.1016/S0031-9201(03)00030-X.

Gudmundsson, Ó., and M. Sambridge (1998). A regionalized upper mantle (RUM) seismic model, *J. Geophys. Res.* **103,** 7121–7136.

Hanks, T. C., and H. Kanamori (1979). A moment magnitude scale, *J. Geophys. Res.* **84,** 2348–2350.

Igarashi, T. (2010). Spatial changes of inter-plate coupling inferred from sequences of small repeating earthquakes in Japan, *Geophys. Res. Lett.* **37,** no. L20304, 5, doi: 10.1029/2010GL044609.

Igarashi, T., T. Matsuzawa, and A. Hasegawa (2003). Repeating earthquakes and interplate aseismic slip in the northeastern Japan subduction zone, *J. Geophys. Res.* **108,** no. 2249, doi: 10.1029/2002JB001920.

Johnson, L. R., and R. M. Nadeau (2002). Asperity model of an earthquake: Static problem, *Bull. Seismol. Soc. Am.* **92,** 672–686.

Kanamori, H., and D. L. Anderson (1975). Theoretical basis of some empirical relations in seismology, *Bull. Seismol. Soc. Am.* **65,** 1073–1095.

Kennett, B. L. N., and E. R. Engdahl (1991). Traveltimes for global earthquake location and phase identification, *Geophys. J. Int.* **105,** 429–465.

Lay, T., C. J. Ammon, H. Kanamori, L. Rivera, K. D. Koper, and A. R. Hutko (2010). The 2009 Samoa–Tonga great earthquake triggered doublet, *Nature* **466,** 964–968, doi: 10.1038/Nature09214.

Li, L., Q. F. Chen, X. Cheng, and F. Niu (2007). Spatial clustering and repeating of seismic events observed along the 1976 Tangshan fault, north China, *Geophys. Res. Lett.* **34,** no. L23309, 6, doi: 10.1029/2007GL031594.

Marone, C., J. E. Vidale, and W. L. Ellsworth (1995). Fault healing inferred from time dependent variations in source properties of repeating earthquakes, *Geophys. Res. Lett.* **22,** 3095–3098.

Matsuzawa, T., T. Igarashi, and A. Hasegawa (2002). Characteristic small-earthquake sequence off Sanriku, northeastern Honshu, Japan, *Geophys. Res. Lett.* **29,** no. 1543, 4, doi: 10.1029/2001GL014632.

Myhill, R., D. McKenzie, and K. Priestley (2011). The distribution of earthquake multiplets beneath the southwest Pacific, *Earth Planet. Sci. Lett.* **301,** nos. 1–2, 87–97, doi: 10.1016/j.epsl.2010.10.023.

Nadeau, R. M., and L. R. Johnson (1998). Seismological studies at Parkfield VI: Moment release rates and estimates of source parameters for small repeating earthquakes, *Bull. Seismol. Soc. Am.* **88,** 790–814.

Nadeau, R. M., and T. V. McEvilly (1999). Fault slip rates at depth from recurrence intervals of repeating microearthquakes, *Science* **285,** 718–721.

Nadeau, R. M., W. Foxall, and T. V. McEvilly (1995). Clustering and periodic recurrence of microearthquakes on the San Andreas fault at Parkfield, California, *Science* **267,** 503–507.

Pacheco, J. F., L. R. Sykes, and C. H. Scholz (1993). Nature of seismic coupling along simple plate boundaries of the subduction type, *J. Geophys. Res.* **98,** 14,133–14,159.

Pelletier, B., S. Calmant, and R. Pillet (1998). Current tectonics of the Tonga–New Hebrides region, *Earth Planet. Sci. Lett.* **164,** 263–276.

Peng, Z. G., and Y. Ben-Zion (2006). Temporal changes of shallow seismic velocity around the Karadere–Düzce branch of the North Anatolian fault and strong ground motion, *Pure Appl. Geophys.* **163,** nos. 2–3, 567–600, doi: 10.1007/s00024-005-0034-6.

Peng, Z. G., J. E. Vidale, C. Marone, and A. Rubin (2005). Systematic variations in recurrence interval and moment of repeating aftershocks, *Geophys. Res. Lett.* **32,** no. L15301, 4, doi: 10.1029/2005GL022626.

Peterson, E. T., and T. Seno (1984). Factors affecting seismic moment release rates in subduction zones, *J. Geophys. Res.* **89,** 10,233–10,248.

Poupinet, G., W. L. Ellsworth, and J. Frechet (1984). Monitoring velocity variations in the crust using earthquake doublets: An application to the Calaveras Fault, California, *J. Geophys. Res.* **89,** 5719–5731.

Rubin, A. M., D. Gillard, and J. L. Got (1999). Streaks of microearthquakes along creeping faults, *Nature* **400,** 635–641.

Rubinstein, J. L., and G. C. Beroza (2004). Evidence for widespread nonlinear strong ground motion in the M_w 6.9 Loma Prieta Earthquake, *Bull. Seismol. Soc. Am.* **94,** 1595–1608.

Rubinstein, J. L., and G. C. Beroza (2005). Depth constraints on nonlinear strong ground motion from the 2004 Parkfield earthquake, *Geophys. Res. Lett.* **32,** no. L14313, 5, doi: 10.1029/2005GL023189.

Rubinstein, J. L., N. Uchida, and G. C. Beroza (2007). Seismic velocity reductions caused by the 2003 Tokachi-Oki earthquake, *J. Geophys. Res.* **112,** no. B05315, 12, doi: 10.1029/2006JB004440.

Sammis, C. G., and J. R. Rice (2001). Repeating earthquakes as low-stress-drop events at a border between locked and creeping fault patches, *Bull. Seismol. Soc. Am.* **91,** 532–537.

Sammis, C. G., R. M. Nadeau, and L. R. Johnson (1999). How strong is an asperity? *J. Geophys. Res.* **104,** 10,609–10,619.

Schaff, D. P., and G. C. Beroza (2004). Coseismic and postseismic velocity changes measured by repeating earthquakes, *J. Geophys. Res.* **109,** no. B10302, 14, doi: 10.1029/2004JB003011.

Schaff, D. P., and P. G. Richards (2004). Repeating seismic events in China, *Science* **303,** 1176–1178.

Schaff, D. P., G. C. Beroza, and B. E. Shaw (1998). Postseismic response of repeating aftershocks, *Geophys. Res. Lett.* **25,** 4549–4552.

Schaff, D. P., G. H. R. Bokelmann, G. C. Beroza, F. Waldhauser, and W. L. Ellsworth (2002). High-resolution image of Calaveras fault seismicity, *J. Geophys. Res.* **107,** no. 2186, 16, doi: 10.1029/2001JB000633.

Thatcher, W., and J. N. Brune (1971). Seismic study of an oceanic ridge earthquake swarm in Gulf of California, *Geophys. J. Roy. Astron. Soc.* **22,** 473–489.

Uchida, N., and T. Matsuzawa (2011). Coupling coefficient, hierarchical structure, and earthquake cycle for the source area of the 2011 off the Pacific coast of Tohoku earthquake inferred from small repeating earthquake data, *Earth Planets Space* **63,** no. 7, 675–679, doi: 10.5047/eps.2011.07.006.

Uchida, N., A. Hasegawa, T. Matsuzawa, and T. Igarashi (2004). Pre- and post-seismic slow slip on the plate boundary off Sanriku, NE Japan associated with three interplate earthquakes as estimated from small repeating earthquake data, *Tectonophysics* **385,** nos. 1–4, 1–15, doi: 10.1016/j.tecto.2004.04.015.

Uchida, N., T. Matsuzawa, A. Hasegawa, and T. Igarashi (2003). Interplate quasi-static slip off Sanriku, NE Japan, estimated from repeating earthquakes, *Geophys. Res. Lett.* **30,** no. 1801, 4, doi: 10.1029/2003GL017452.

Uchida, N., T. Matsuzawa, W. L. Ellsworth, K. Imanishi, T. Okada, and A. Hasegawa (2007). Source parameters of a M 4.8 and its accompanying repeating earthquakes off Kamaishi, NE Japan: Implications for the hierarchical structure of asperities and earthquake cycle, *Geophys. Res. Lett.* **34,** no. L20313, 5, doi: 10.1029/2007GL031263.

Uchida, N., S. Yui, S. Miura, T. Matsuzawa, A. Hasegawa, Y. Motoya, and M. Kasahara (2009). Quasi-static slip on the plate boundary associated with the 2003 M 8.0 Tokachi-oki and 2004 M 7.1 off-Kushiro earthquakes, Japan, *Gondwana Res.* **16,** nos. 3–4, 527–533, doi: 10.1016/j.gr.2009.04.002.

Uchida, N., J. Nakajima, A. Hasegawa, and T. Matsuzawa (2009). What controls interplate coupling?: Evidence for abrupt change in coupling across a border between two overlying plates in the NE Japan subduction zone, *Earth Planet. Sci. Lett.* **283,** nos. 1–4, 111–121, doi: 10.1016/j.epsl.2009.04.003.

Uyeda, S., and H. Kanamori (1979). Back-arc opening and the mode of subduction, *J. Geophys. Res.* **84,** 1049–1061.

Vidale, J. E., W. L. Ellsworth, A. Cole, and C. Marone (1994). Variations in rupture process with recurrence interval in a repeated small earthquake, *Nature* **368,** 624–626.

Waldhauser, F., and W. L. Ellsworth (2000). A double-difference earthquake location algorithm: Method and application to the northern Hayward fault, California, *Bull. Seismol. Soc. Am.* **90,** 1353–1368.

Wen, L. (2006). Localized temporal change of the Earth's inner core boundary, *Science* **314,** no. 5801, 967–970, doi: 10.1126/science.1131692.

Wessel, P., and W. H. F. Smith (1998). New, improved version of the Generic Mapping Tools released, *Eos Trans. AGU* **79,** 579.

Wiens, D. A., and N. O. Snider (2001). Repeating deep earthquakes: Evidence for fault reactivation at great depth, *Science* **293,** 1463–1466.

Yu, W., and L. Wen (2012). Deep-focus repeating earthquakes in the Tonga–Fiji subduction zone, *Bull. Seismol. Soc. Am.* **102,** no. 4, 1829–1849, doi: 10.1785/0120110272.

Zhang, J., P. G. Richards, and D. P. Schaff (2008). Wide-scale detection of earthquake waveform doublets and further evidence for inner core super-rotation, *Geophys. J. Int.* **174,** no. 3, 993–1006, doi: 10.1111/j.1365-246X.2008.03856.x.

Zhang, J., X. D. Song, Y. C. Li, P. G. Richards, X. L. Sun, and F. Waldhauser (2005). Inner core differential motion confirmed by earthquake waveform doublets, *Science* **309,** no. 5739, 1357–1360, doi: 10.1126/science.1113193.

Zhao, P., and Z. G. Peng (2009). Depth extent of damage zones around the central Calaveras fault from waveform analysis of repeating earthquakes, *Geophys. J. Int.* **179,** no. 3, 1817–1830, doi: 10.1111/j.1365-246X.2009.04385.x.

Institute of Earth Sciences
Academia Sinica
No. 128 Section 2 Academia Road, Nangang
Taipei 11529, Taiwan
fgsyw@earth.sinica.edu.tw

Manuscript received 31 March 2012